Interplay between Passive Tension and Strong and Weak Binding Cross-Bridges in Insect Indirect Flight Muscle

A Functional Dissection by Gelsolin-mediated Thin Filament Removal

HENK L. M. GRANZIER and KUAN WANG

From the Clayton Foundation Biochemical Institute, Department of Chemistry and Biochemistry, University of Texas at Austin, Austin, Texas 78712

ABSTRACT The interplay between passive and active mechanical properties of indirect flight muscle of the waterbug (*Lethocerus*) was investigated. A functional dissection of the relative contribution of cross-bridges, actin filaments, and C filaments to tension and stiffness of passive, activated, and rigor fibers was carried out by comparing mechanical properties at different ionic strengths of sarcomeres with and without thin filaments. Selective thin filament removal was accomplished by treatment with the actin-severing protein gelsolin. Thin filament removal had no effect on passive tension, indicating that the C filament and the actin filament are mechanically independent and that passive tension is developed by the C filament in response to sarcomere stretch. Passive tension increased steeply with sarcomere length until an elastic limit was reached at only 6–7% sarcomere extension, which corresponds to an extension of 350% of the C filament. The passive tension–length relation of insect flight muscle was analyzed using a segmental extension model of passive tension development (Wang, K., R. McCarter, J. Wright, B. Jennate, and R. Ramirez-Mitchell. 1991. *Proc. Natl. Acad. Sci. USA.* 88:7101–7109). Thin filament removal greatly depressed high frequency passive stiffness (2.2 kHz) and eliminated the ionic strength sensitivity of passive stiffness. It is likely that the passive stiffness component that is removed by gelsolin is derived from weak-binding cross-bridges, while the component that remains is derived from the C filament. Our results indicate that a significant number of weak-binding cross-bridges exist in passive insect muscle at room temperature and at an ionic strength of 195 mM. Analysis of rigor muscle indicated that while rigor tension is entirely actin based, rigor stiffness contains a component that resists gelsolin treatment and is therefore likely to be C filament based. Active tension and active stiffness of unextracted fibers were directly proportional to passive tension before activation. Similarly, passive stiffness due to

Address reprint requests to Dr. Kuan Wang, Department of Chemistry and Biochemistry, University of Texas at Austin, Austin, TX 78712.

J. GEN. PHYSIOL. © The Rockefeller University Press · 0022-1295/93/02/0235/36 $2.00
Volume 101 February 1993 235–270

weak bridges also increased linearly with passive tension, up to a limit. These correlations lead us to propose a stress–activation model for insect flight muscle in which passive tension is a prerequisite for the formation of both weak-binding and strong-binding cross-bridges.

INTRODUCTION

Tension and stiffness of passive striated muscle have gained increasing attention in recent years due to the discovery of a family of giant filamentous proteins, titin and minititin, that are involved in the development of passive tension (for reviews see Wang, 1985; Maruyama, 1986; Trinick, 1991). In vertebrate skeletal and cardiac muscle each titin molecule is ~1 μm long and 2.5–3.0 MD in mass and spans from the Z line to the M line region of the sarcomere. The titin segment in the I band is extensible and acts as an elastic connector that develops passive tension when the sarcomere is stretched. The remaining titin segment in the A band associates with the myosin filament and is normally prevented from extension. This anchored A segment, however, can be recruited to contribute to passive tension when structural constraints are relieved; e.g., in sarcomeres that have been stretched beyond their elastic limit (Wang, McArter, Wright, Jennate, and Ramirez-Mitchell, 1991, 1993) or in sarcomeres from which myosin filaments have been selectively extracted (Higuchi, Suzuki, Kimura, Yoshioka, Maruyama, and Umazuma, 1992).

The segmental organization of titin formed the basis for a proposed segmental extension model of passive tension (Wang et al., 1991, 1993). The model is able to account for the basic shape of the passive tension–sarcomere length relation, for the change in this relation in muscles that have been stretched beyond their elastic limit, and for the variation of tension–length relations of muscles that express different titin size variants (Wang et al., 1991, 1993). The passive tension of the extensible segment of titin is also important in keeping the A band in the center of the sarcomere (Horowits and Podolsky, 1987).

Invertebrate muscles express proteins that are analogous to vertebrate titin: minititin, twitchin, and projectin, with reported sizes from 0.6 to 1.2 MD (Benian, Kiff, Neckelman, Moerman, and Waterston, 1989; Hu, Mutsuno, Terakado, Matsuura, Kimura, and Maruyama, 1990; Lakey, Ferguson, Labeit, Reedy, Larkins, Butcher, Leonard, and Bullard, 1990; Nave and Weber, 1990; Ayme-Southgate, Vigoreaux, Benian, and Pardue, 1991; Nave, Furst, Vinkemeier, and Weber, 1991). Minititin, found in insect indirect flight muscle, is 260 nm long and is localized between the Z line and the outer region of the A band (Nave and Weber, 1990). Minititin is thought to constitute the connecting filaments (C filaments) that connect the end of the thick filaments to the Z lines (Reedy, 1971; White and Thorson, 1973; Trombitás and Tigyi-Sébes, 1979). Minititin may serve roles in the development of passive tension, A band centering, and the stretch-activation mechanism of insect indirect flight muscle (for reviews see Pringle, 1978; Tregear, 1983).

While titin and minititin are likely to contribute to dynamic stiffness of stretched passive muscle, the contribution of actomyosin interaction to stiffness has also been recognized (Moss, Sollins, and Julian, 1976; Brenner, Schoenberg, Chalovich, Greene, and Eisenberg, 1982; Brenner, Chalovich, Greene, Eisenberg, and Schoenberg, 1986; Brenner, Yu, and Chalovich, 1991; Schoenberg, 1988). Cross-bridges

that interact with actin in passive vertebrate muscle are commonly referred to as weak-binding cross-bridges (weak bridges), and are characterized by low actin affinity and rapid attachment/detachment that is very sensitive to temperature and ionic strength. As a result of their kinetic properties, weak bridges contribute to high frequency stiffness, but not to tension. So far, weak bridges in vertebrate muscle have only been conclusively demonstrated at low temperature (~5°C) and low ionic strength (~20 mM). Nevertheless, it is thought that these weak bridges are essential precursors for force-generating, strongly binding cross-bridges (strong bridges) under physiological conditions (Brenner et al., 1991). Despite the well-known high passive stiffness of insect indirect flight muscle (Pringle, 1977), the relative contributions of weak bridges and minititin to the total stiffness remain open.

We report our studies on passive and active mechanical properties of indirect flight muscle of the waterbug (*Lethocerus*), focusing especially on their interplay, which leads to stretch activation, and the possible structural and molecular bases of these properties. Experimentally, a functional dissection of the relative contribution of cross-bridges, actin filaments, and C filaments to tension and stiffness of passive, activated, and rigor fibers was achieved by comparing mechanical properties at different ionic strengths and before and after selective removal of thin filaments. Thin filament removal was achieved by applying the technique of Funatsu, Higuchi, and Ishiwata (1990), which makes use of the actin filament–severing activity of gelsolin.

We observed that thin filament removal had no effect on passive tension, indicating that the C filament and the actin filament are mechanically independent. Actin extraction, however, greatly depressed passive stiffness and eliminated the ionic strength sensitivity of passive stiffness. It appears that weak bridges exist in significant numbers in passive insect muscle at room temperature and physiological ionic strength. Further mechanical studies of thin filament free sarcomeres indicated that the C filament is mainly, if not exclusively, responsible for passive tension development and contributes significantly to passive stiffness and rigor stiffness of insect flight muscle. Active tension in unextracted fibers is directly proportional to the passive tension level before activation. Similarly, passive stiffness due to weak bridges also increases linearly with passive tension, up to a limit. These correlations lead us to propose a stress-activation model for insect flight muscle in which passive tension is a prerequisite for the formation of both weak and strong cross-bridges.

MATERIALS AND METHODS

Fiber Bundles

The dorso-longitudinal muscle (DLM) of the waterbug was studied. Experiments in which fresh and glycerinated fibers were compared were done with *Lethocerus griseus* and *Lethocerus uhleri* from Florida, while all other experiments used *Lethocerus indicus* from Thailand. Waterbugs were kept in an aquarium for up to 6 mo and fed small live fish. The bugs were first immobilized on ice and then wings, legs, head, and abdomen were quickly removed. A large volume (25 ml) of solution A (10 mM KCl, 100 mM NaCl, 5 mM $MgCl_2$, 10 mM Na phosphate, 2 mM diisopropylfluorophosphate (DIFP), 0.5 mM phenylmethenesulfonyl fluoride (PMSF), and 20 μg/ml leupeptin, pH 7.0, at 4°C) was immediately squirted through the thorax cavity to wash away and inhibit digestive tract enzymes. The DLM was exposed by cutting both the

ventral chitin and dorso-ventral muscles using small scissors, washed extensively with solution A, and then soaked for 20 min in 40 ml of solution A to allow protease inhibitors to penetrate. A small bundle of ~100 fibers was removed and used immediately for experimentation, while the remaining muscle was glycerinated for later use.

Glycerination was done according to Reedy, Leonard, Freeman, and Arad (1981; and Reedy, M.K., personal communication) by alternately soaking the muscle for 2 h in 40 ml of relaxing solution B (20 mM K phosphate, 10 mM EGTA, 6.4 mM $MgAc_2$, 5.9 Na_2ATP, 5 mM NaN_3, 1 mM DTT, 0.5 mM PMSF, and 20 μg/ml leupeptin, pH 7.0 at 4°C) and then for 2 h in 40 ml of relaxing solution C (solution B containing 50% (vol/vol) glycerol). The first two times solution B contained 1% (wt/vol) of purified Triton X-100 (28314; Pierce Chemical Co., Rockford, IL) and 3 mM DIFP. Two additional cycles (total of four cycles) of soaking were done in solutions B and C without additives. Finally, the muscle was soaked in 40 ml of solution C for 4 h (the solution was replaced after 2 h). Small fiber bundles were dissected, transferred into 1-ml tubes containing solution C, stored at −20°C, and used for up to two months after the muscle was glycerinated.

Dissection and glycerination were carried out at 4°C. During glycerination the muscle was added to a 40-ml centrifuge tube filled with solution and tumbled on a vertical rotator (at 10 rpm). To avoid calcium contamination and activation of calcium-dependent proteases, all dissection tools and containers were washed with 500 mM EGTA (pH 7.6) and then rinsed with relaxing solution B.

Single Fibers

Fiber bundles (in solution A for fresh fibers and solution C for glycerinated fibers) were transferred to relaxing solution (D in Table I) in a petri dish that contained a Sylgard dissection base (182 silicone elastomere; Dow Corning Corp., Midland, MI). Single fibers were separated and pinned down by stainless steel pins (100 μm in diameter) and then skinned. First the fibers were chemically skinned by changing the bathing solution to solution D containing 0.5% (wt/vol) Triton X-100. This step solubilized mitochondria and facilitated subsequent mechanical skinning which was achieved by grasping a few surface myofibrils and then pulling them gently away. The fibers were soaked in Triton-containing solution D for a total of 30 min and then washed extensively with solution D.

To mount fibers in the mechanical setup, a small T-shaped aluminum clip was glued to each end of the fiber as follows. A small hole was punched in the base of the clip with a pin while the sides of the upper part of the T clip were folded upward and a small amount (< 1 μl) of cyanoacrylic glue was placed in their center with the aid of a tiny loop that was made from a 100-μm-thick needle. The T clip was then positioned to the very edge of a depression in the Sylgard dissection base that was filled with relaxing solution D, in which the fiber was free-floating. One end of the fiber was pulled out of the solution for a very short distance such that the end was submerged in the glue. A large amount of solution D was immediately added to the dissection dish, submerging the T clip and causing rapid hardening of the glue (< 5 s). Finally, the upper part of the T clip was folded and pressed on the hardened glue that embedded the end of the fiber. The other end of the fiber was glued next to another clip. The strength of the fiber-clip attachment appeared adequate since fibers could be mounted via these clips and stretched and activated repeatedly without noticeable change in fiber slack length and thus without permanent "give" at the attachment sites. Plots of fiber-strain (fiber length measured from clip to clip) versus sarcomere-strain (see below) were found to be linear with a slope of 1.0, indicating again that the ends were glued firmly and that sarcomeres between the clips stretched uniformly.

Mechanics Setup

The setup is shown schematically in Fig. 1. A small (50 μl) quartz chamber was mounted on an XY stage of an inverted microscope (M100 PF; Swift Instruments Inc., San Jose, CA). A servomotor (300S; Cambridge Technology, Inc., Cambridge, MA) and a force transducer (AME 801E; Aksjeselskapet Mikro-electronic, Horten, Norway) were mounted to miniature XYZ manipulators on the stage. The servomotor had a small L-shaped platinum hook (200 μm in diameter) glued to its arm, while the force transducer had a similar hook glued to the end of its beam. The fiber was mounted horizontally to these hooks using the T clips glued to the ends.

TABLE I

Solution Composition

	Relaxing D	Activating E	Rigor F	Low μ relaxing G
Imidazole (mM)	40	40	40	40
K_2 EGTA (mM)	10	0	10	2
K_2 Ca EGTA (mM)*	0	10	0	0
Mg acetate (mM)	6.4	6.3	1	3.6
Na_2ATP (mM)	5.9	6.0	0	3
K propionate (mM)	0 (65)‡	0	30	0 (85)‡
NaN_3 (mM)	5	5	5	1
DTT (mM)	1	1	1	1
Na_2CP (mM)	15	15	0	2
CPK (U/ml)	100	100	0	100
Leupeptin (μg/ml)	20	20	20	20
pH (21–23°C)	6.8	6.8	6.8	6.8
μ (mM)§	130 (195)‡	129	90	45 (130)‡
pCa§	9.25	4.25	9.25	8.8
MgATP (mM)§	5	5	0	2.5
Mg^{2+} (mM)§	1.0	1.0	1.0	1.0

EGTA, ethyleneglycol-bis-(β-aminoethylether) *N,N,N',N'*-tetraacetic acid (Ca and Mg chelator); ATP, adenosine 5'-triphosphate; DTT, dithiothreitol (reducing agent); CP, creatine phosphate; CPK, creatine-phosphokinase (to regenerate ATP); DIFP, diisopropylfluorophosphate (protease inhibitor); PMSF, phenyl-methenesulfonyl fluoride (protease inhibitor).

*Obtained by mixing equimolar concentrations of EGTA and $CaCO_3$ and heating at 80°C until CO_2 production ceased (~10 min).

‡For experiments in which the effect of ionic strength on passive stiffness was studied, we used solutions D, G, a high ionic strength relaxing solution (μ = 195 mM) prepared by adding 65 mM K propionate to solution D, and a second μ = 130 mM relaxing solution obtained by adding 85 mM K propionate to solution G.

§Free and total concentrations were computed on an IBM AT computer using the program published by Fabiato (1988). The apparent binding constants and charges of the metal–ligand complexes were calculated for a pH of 6.8 at 22°C. Ionic strength, μ, was calculated from solution composition and the measured amount of KOH used to adjust pH. For pCa calculation, a calcium contamination of 5 μM was assumed.

Sarcomere length was measured with laser diffraction using a 0.8-mm-wide He-Ne laser beam (106-2; Spectra-Physics Analytical, San Jose, CA); the diffraction pattern was collected with a long working distance objective (ELWD #327800, ×40; Nikon Inc., Melville, NY). A telescope lens (MA 690; Swift Instruments Inc.) was focused on the back focal plane of the objective and the diffraction pattern was projected, after compression with a cylindrical lens, onto a photo diode array (RL 256 C/17; EG&G Reticon, Sunnyvale, CA). The first-order diffraction peak position was obtained from the median position of the first-order intensity

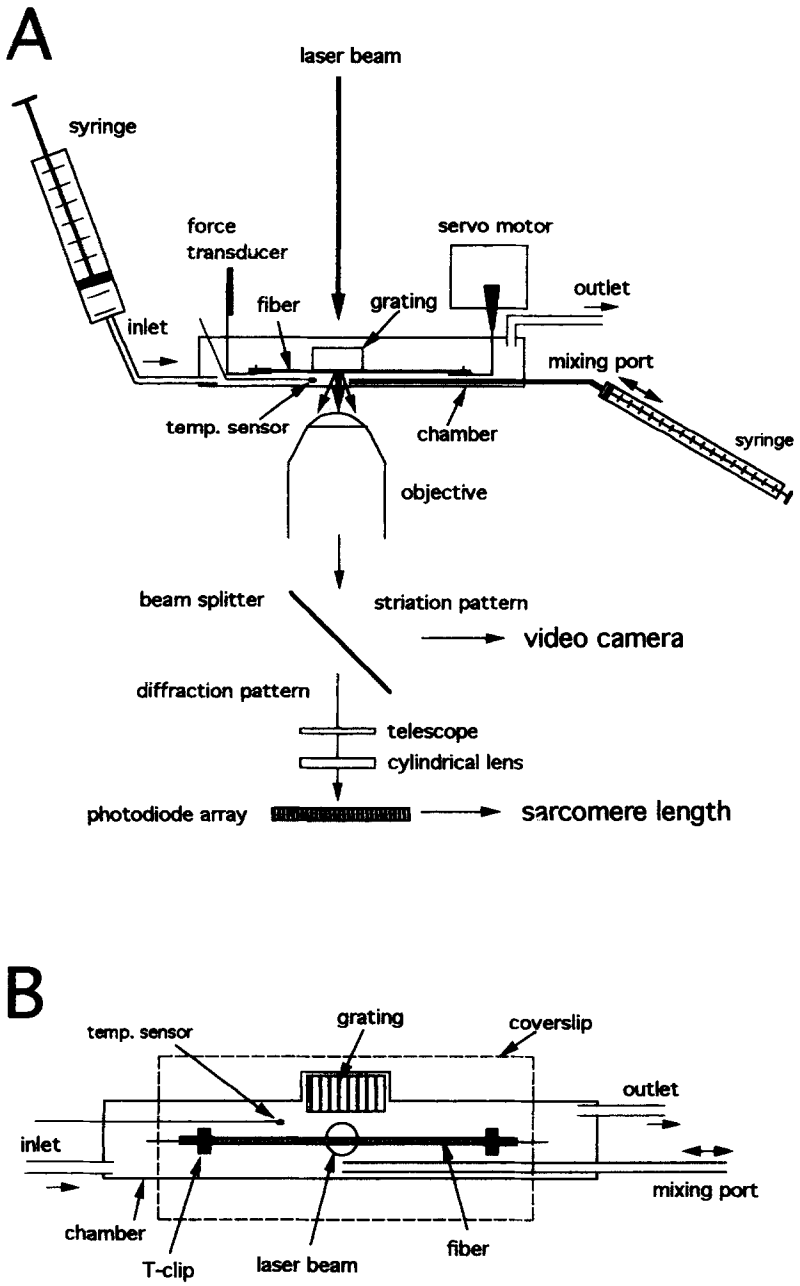

FIGURE 1. Mechanics setup. (*A*) Side view of setup; (*B*) top view of chamber. See Materials and Methods for further details.

profile according to Granzier, Myers, and Pollack (1987). This position signal was digitized (see below) and converted to sarcomere length using a calibration curve that was established with the 6th through 13th diffraction peaks of a 25-μm grating (A38,260; Edmund Scientific Co., Barrington, NJ) that was present in the chamber (Fig. 1).

The sarcomere length signals of insect fibers were generally weak, but usable, with peak-peak noise of typically 5 nm/sarcomere. The same instrumentation resulted in low noise signals (< 1 nm per sarcomere) when used on rabbit psoas fibers (Granzier and Wang, 1993). This high sarcomere noise level of insect fibers probably resulted from a number of factors, such as the smaller fiber diameter, the low number of myofibrils per fiber, and the very high content of mitochondria (Pringle, 1965). In a few cases where the intensity of the diffraction pattern was below the detection limit of the photodiode array, the fiber length signal was used to correlate with mechanics (only Fig. 12 represents such a compromise).

Solution exchange was achieved by rapidly injecting new solution from an inlet at one end of the chamber and withdrawing it from the outlet positioned diagonally across the chamber (Fig. 1). The efficiency of solution exchange was determined in pilot experiments by monitoring absorbance of ATP after solution exchange. After injecting 0.3 ml of relaxing solution (in ~1 s) in the chamber that contained rigor solution, the ATP concentration in the chamber reached 96% of the level of the relaxing solution. During actual experiments fibers were activated by injecting 1 ml of activating solution (E in Table I) into the chamber in 1–3 s. To induce rigor, 10 ml of solution F was injected in 1 min. Fibers were relaxed again by adding 2 ml of relaxing solution (D). A small coverslip was placed on top of the filled chamber (Fig. 1 *B*) so that the fiber could be imaged without distortion caused by an uneven solution surface. The coverslip also reduced evaporation to the point that it took at least 30 min before the chamber content noticeably reduced in volume (by ~5 μl). Nevertheless, the solution was replaced every 10 min throughout the course of the experiment to ensure consistency of solution composition.

The chamber also contained a mixing port that was connected to a 10 μl syringe (Fig. 1) for use during gelsolin treatment. A small amount of solution was withdrawn from near the center of the fiber and then quickly reinjected for mixing and preventing of diffusion gradients. Finally, there was also a small temperature sensor (J-type; 25 μm in diameter; Omega Engineering Inc., Stamford, CT) mounted in the chamber.

Root mean square (RMS) force noise was 2 μN; the compliance of the transducer and its hook was 5 nm/μN and the resonance frequency was 3,300 Hz. RMS position detector noise of the servomotor was 0.3 μm and the compliance of the servomotor and hook was 1 nm/μN. The −3 dB frequency of the servomotor was 800 Hz. When high frequencies were used in this work, the amplitude of the input signal was varied such that a constant output amplitude was obtained at all frequencies (see correction factors below).

Mechanics Protocols

In the basic stretch protocol the relation between passive tension and sarcomere length was measured (Fig. 2 *A*). The fiber was stretched with a constant rate (which in different experiments ranged from 0.01 to 0.05% slack length/s) to a predetermined amplitude (range from 0.5 to 5%) and held at this length for a specified duration (range from 50 to 260 s). Subsequently, the fiber was either stretched again or released to its initial length. Every 350 ms, fiber length, sarcomere length, and tension were measured (with a delay of 0.008 ms). To allow stress-relaxation to take place, the values reached just before the next stretch-release (Fig. 2 *A*, double-headed arrows) were used for plotting length–tension loops (e.g., Fig. 2 *B*).

In the constant frequency protocol the complex stiffness–sarcomere length relation was measured. Dynamic stiffness was obtained with small amplitude length oscillations (Kawai and Brandt, 1980). The fiber was subjected to brief 15-ms bursts of high frequency sinusoidal length oscillations that were repeated every 350 ms (2.2 kHz; amplitude 0.1%) while being stretched

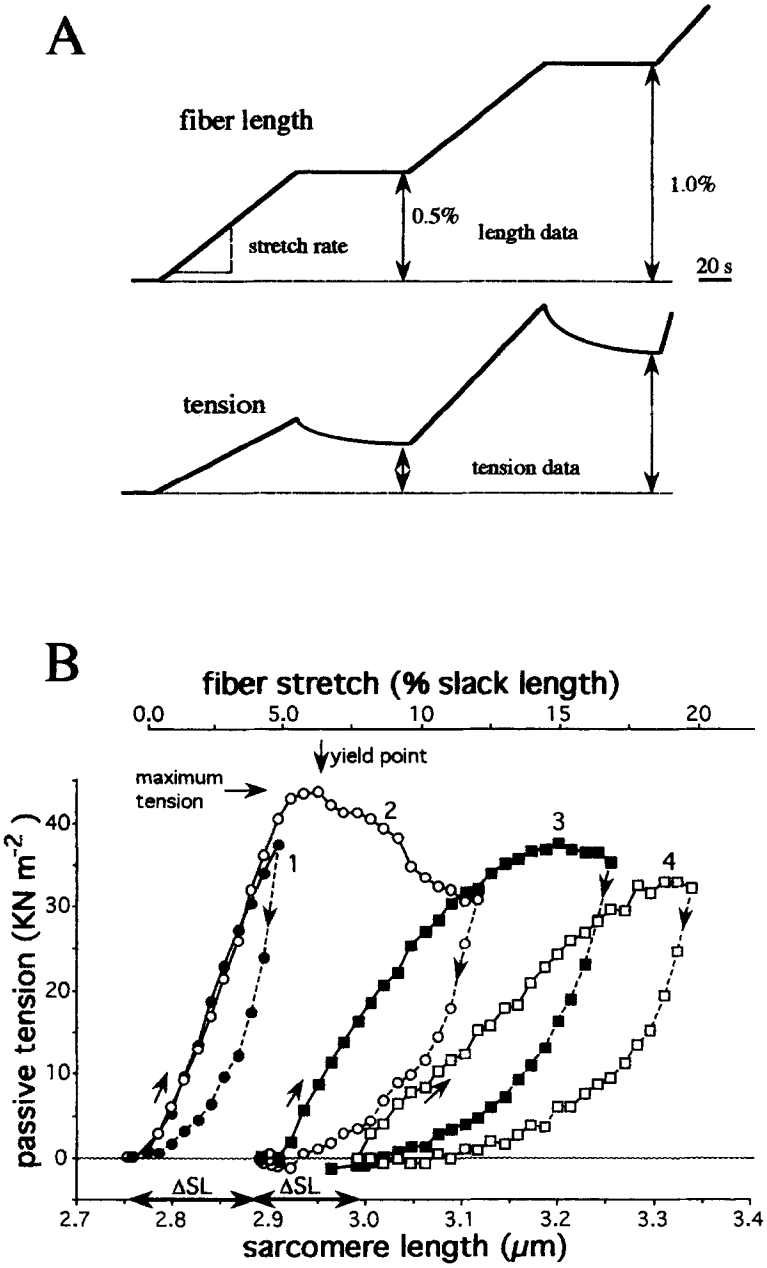

FIGURE 2. Passive tension–sarcomere length loops of fresh fiber in relaxing solution. (*A*) The fiber was stretched with a constant rate (0.05%/s) to a predetermined amplitude (0.5%) and held at this length for a specified duration (80 s), after which the fiber was stretched again. Every 350 ms, fiber length, sarcomere length, and tension were measured. The values reached just before the next stretch/release (double-headed arrows) were used for plotting length–tension loops. (*B*) Tension–length loops. This fiber was subjected to four cycles of stretch and release with a 20-min rest period in between. The total degree of stretch was increased in subsequent cycles. If sarcomeres were stretched beyond the yield point, subsequent tension–length loops had reduced slopes and longer slack lengths. These findings on fresh fibers are similar to those reported on glycerinated fibers by White (1983). See test for further details.

by the basic stretch protocol (Fig. 3 *A*). Each burst consisted of 32 oscillations (generated digitally and converted to analog with a conversion time of 28 μs). The ensuing tension oscillations were sampled (analog-to-digital conversion time: 7 μs; 64 samples/oscillation), and the tension amplitude was determined with fast Fourier transform (FFT) analysis. Complex stiffness was calculated as the ratio of tension amplitude to strain amplitude (top of Fig. 3 *B*). FFT analysis is rapid and allows phase information to be obtained simultaneously (see below). Stiffness was measured every 350 ms, thus allowing the time course of stiffness change to be monitored (e.g., Fig. 3 *A*, bottom signal). Stiffness measurements were carried out every 10 ms after length and tension were sampled. Hence, oscillations in length and tension during stiffness measurement were not represented in tension traces (Fig. 3 *A*). Stiffness values attained just before the next stretch-release were used to plot stiffness–sarcomere length curves (Fig. 8, bottom right panel; Figs. 11 *B* and 12 *B*).

In the frequency sweep protocol the complex stiffness and phase angle were measured at a wide range of frequencies (Fig. 3). The protocol was similar to the constant frequency protocol, except that at a predetermined time the frequency was varied from 2,500 Hz down to 0.1 Hz (amplitude typically 0.1%). The sweep consisted of a total of 50 different frequencies with a 0.25-s rest period in between individual frequencies. The servomotor position signal and tension were digitized and their amplitudes and phases were determined (Fig. 3 *B*) with FFT analysis. The values for a given frequency were first calculated during the 0.2-s rest period and at the end of the frequency sweep all values were corrected within 20 s for instrument modulation. Further details can be found in Fig. 3.

Stiffness and Phase Correction

Measurements were corrected for several sources of modulation that were instrument based. The first source was from the force amplifier electronics that caused phase shift and amplitude roll-off of the force signal. These characteristics were determined by replacing the force transducer with matched 1-kΩ resistors and loading them with a sinusoidally varying voltage (amplitude 1 V). The second modulation resulted from the force transducer element. Its phase shift and amplitude roll-off were determined by gluing a 50-mm-long, 20-μm-thick Ni-Chrome wire between servomotor and force transducer hooks, imposing a frequency sweep (amplitude 0.5 μm), and assuming that the wire itself behaved elastically at all frequencies. The transducer characteristics were confirmed on several occasions by using muscle fibers that were in rigor and then fixed with 2.5% glutaraldehyde (cf. Kawai and Brandt, 1980). The third source of modulation was a phase shift of the data acquisition system, which used a single analog-to-digital converter that was multiplexed. The phase shift was measured by sampling identical signals simultaneously by all channels. The fourth source was from the position detector of the servomotor that contained an RC filter with a −3-dB frequency of 30 kHz. The phase shift and amplitude roll-off of this filter were computed.

Amplitude corrections were done by multiplying values measured during the experiment by the inverse of the roll-off for each of the sources of modulation, while phase correction was by appropriate subtraction and addition of phases. Amplitude modulation by acquisition system and servomotor electronics was found to be less than the noise level and was ignored. Blank coupling (i.e., force transmission from servomotor to force transducer independent of muscle fiber) was also corrected. This was measured for each experiment by removing the fiber from the chamber and imposing a frequency sweep. Fig. 4 shows that the net correction factors were small for frequencies lower than ~100 Hz, but became significant at higher frequencies (the magnitude at 1,000 Hz is indicated in Fig. 4).

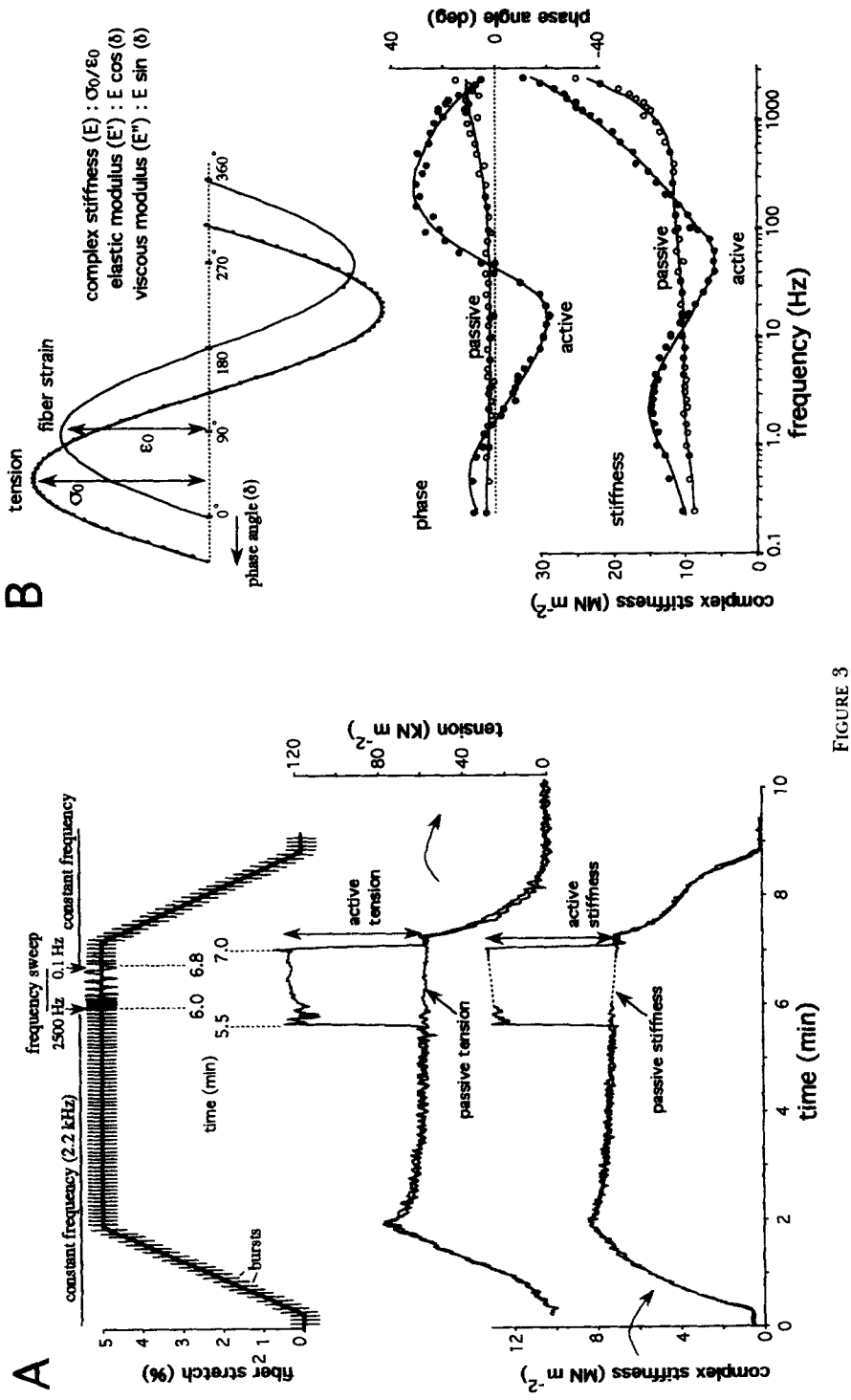
A
fiber stretch (%)
constant frequency (2.2 kHz)
frequency sweep
2500 Hz 0.1 Hz
constant frequency
bursts
time (min)
5.5
6.0
6.8
7.0
tension (KN m-2)
active tension
passive tension
active stiffness
passive stiffness
complex stiffness (MN m-2)
time (min)
B
tension
fiber strain
σ0
ε0
0°
90°
180°
270°
360°
phase angle (δ)
complex stiffness (E) : σ0/ε0
elastic modulus (E') : E cos (δ)
viscous modulus (E") : E sin (δ)
phase angle (deg)
phase
passive
active
stiffness
passive
active
complex stiffness (MN m-2)
frequency (Hz)

FIGURE 3

Hardware and Software

To obtain reproducible passive tension–length curves, fibers were subjected to stretch and release cycles generated by a computer-controlled mechanics workstation that was built to impose identical mechanical protocols. The system contained 16-bit D/A and 16-bit A/D converters, which allowed very slow stretch rates to be imposed and small amplitude signals to be sampled. All three mechanical protocols were generated using an IBM AT computer and a fast acquisition board (DT 2823; Data Translation Inc., Marlboro, MA) with a 100-kHz throughput. Force, fiber length, and sarcomere length (first-order position) were recorded using another IBM AT computer and another acquisition board (DT 2823). By matching D/A and A/D conversion rates for sinusoid generation and data acquisition, and appropriate hand-shaking, an integral number of cycles were sampled. Amplitudes and phases were determined from the first harmonic of the FFT of the servomotor position signal and the force signal.

Software for the protocols, data acquisition, and corrections discussed above, and the sarcomere length determination from both the first-order diffraction peak position and the calibration curve was written using Asyst (Version 3.0; Asyst Software Technologies, Rochester, NY).

Gelsolin Purification

Gelsolin was purified from human plasma according to Bryan (1988), with an additional gel filtration step to remove contaminating lipoprotein (Kruger, Wright, and Wang, 1991). DEAE-purified gelsolin (30 mg from 1 liter of plasma) was applied to a Sephacryl S200 column (2.5 × 80 cm in 25 mM Tris-Cl, 1 mM EGTA, 800 mM NaCl, pH 8.5, at 4°C). The gelsolin fractions were pooled and half was dialyzed into a calcium rigor buffer (170 mM KCl, 10 mM MOPS, 1 mM $MgCl_2$, 0.1 mM $CaCl_2$, 2 mM DIFP, 2 mM leupeptin, pH 7.0 at 20°C) and the other half into a contracting solution (150 mM KCl, 5 mM $MgCl_2$, 4 mM Na_2ATP, 10 mM MOPS, 0.1 mM $CaCl_2$, 2 mM DIFP, 2 mM leupeptin, pH 7.0, at 20°C). The solution (0.3 mg/ml) was then aliquotted into 0.5-ml fractions that were quick-frozen in liquid nitrogen and stored at −70°C.

Gelsolin Treatment of Fibers and Myofibrils

Thin filament removal by gelsolin treatment was as follows. First, ~10 ml of Ca-rigor solution (see above) was added to the chamber until rigor tension and high frequency stiffness reached

---

Figure 3 (*opposite*). Active tension and frequency dependence of stiffness and phase angle of activated and passive fresh fiber. (*A*) Frequency sweep protocol. The fiber at slack length was stretched 5%, held constant, and then released back to its starting length. Each vertical thin line denotes a 15-ms burst of oscillations used to measure complex stiffness at 2.2 kHz (see text for further details). From t = 6 min to t = 6.8 min, a frequency sweep was imposed during which the frequency of oscillation was varied from 2,500 Hz to 0.1 Hz (result shown in *B*). Results of two stretch and release cycles are shown superimposed. One cycle was done in relaxing solution (solution D in Table I). In the other cycle the relaxing solution was replaced at 5.5 min by activating solution (solution E in Table I). The fiber was then relaxed again at t = 7 min and released to its initial length 20 s later. Upon activation both tension and stiffness (2.2 kHz) increased greatly (see two bottom traces). (*B*) Frequency dependence of stiffness and phase angle. Top diagram defines stiffness, phase, elastic modulus, and viscous modulus. Bottom diagram shows frequency dependence of phase and complex stiffness. Characteristics described for activated glycerinated fibers (Thorson and White, 1983; Tregear, 1983) such as negative phase angle (i.e., tension lags length) can be seen in this fresh fiber.

a plateau. Gelsolin (0.3 mg/ml in Ca-rigor buffer) was then added. Rigor tension and rigor stiffness fell rapidly and reached a low constant value typically within ~10 min. The fiber was extensively washed with ~10 ml relaxing solution D (Table I), treated with gelsolin in activating solution (see above) for 5 min, and washed with relaxing solution D for 30 min to remove severed actin filaments.

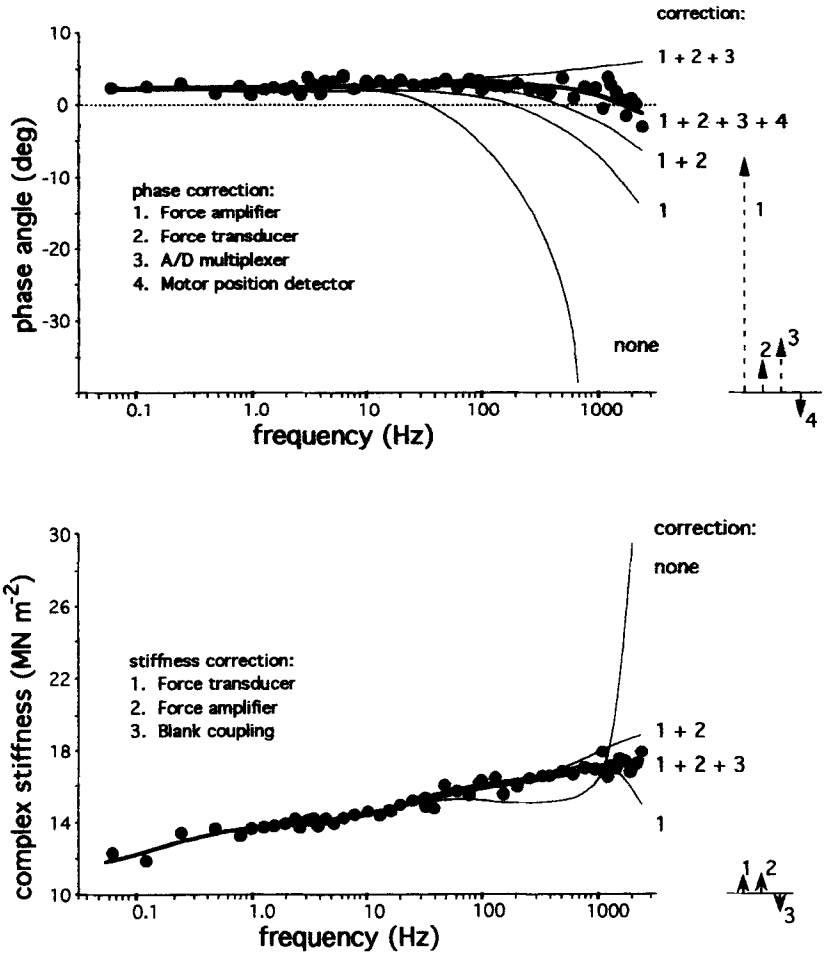

FIGURE 4. Stiffness and phase corrections. The frequency sweep protocol was imposed on a fresh fiber in rigor (solution F) at slack length (sarcomere length 2.60 μm). Filled symbols indicate values that had been fully corrected; the curves (fifth-order polynomial fits) represent the results at various stages of correction. The magnitude and sign of each correction at 1,000 Hz is plotted as arrows to the right. See text for further details.

Gelsolin treatment was also carried out on myofibrils that were prepared from glycerinated muscle. Fiber bundles were minced with a small scalpel and passed twice through each of the three syringe needles used (16-, 21-, and 23-gauge, 1 in. long). The mince was spun in a clinical centrifuge at top speed for 10 min (model CL; International Equipment Co., Needham Heights, MA). Myofibrils in the loose pellet were gently resuspended in rigor solution (F), spun,

and resuspended again. The suspension contained long straight myofibrils that had distinct A and I bands in phase contrast microscopy. Myofibril suspension (40 μl) was settled onto glass coverslips (acid washed and alcohol cleaned) in a moisture box for 1 h. The gelsolin treatment was then performed by adding solutions to the top of the coverslip in a moisture box. The extraction times in both Ca-rigor solution and activating solution were varied from 30 s to 10 min. The extent of thin filament removal was assayed by fluorescent staining with 0.17 μM rhodamine-phalloidin (R-512; Molecular Probes, Inc., Eugene, OR) dissolved in relaxing solution D. The myofibrils were incubated for 1 h, washed in relaxing solution, and observed with an optical microscope (Universal; Carl Zeiss, Inc., Thornwood, NY) equipped with both phase and fluorescence optics (objective lens: ×100; NA 1.2).

Gel Electrophoresis and Gel Staining

After the mechanical experiment, fibers were analyzed with SDS-PAGE. The fibers were presoaked for 60 s in a low ionic strength solution (5 mM Tris-Cl, 0.5 mM DTT, 0.5 mM EGTA, and 2 μg/ml leupeptin, pH 8.4 at 25°C) to enhance solubility of proteins in the megadalton range (Granzier and Wang, 1992). A single fiber (in 10 μl of soaking solution) was quickly injected into 20 μl of 1.5× concentrated stock of Laemmli (1970) sample buffer (50 mM Tris-Cl, 2% SDS, 10% glycerol, 80 mM DTT, and 30 μl/ml Pyronin Y, pH 6.8, at 25°C) that was preheated to 60°C in a water bath. The solution was vigorously mixed for 60 s in the bath and then removed to cool down at room temperature. The sample was centrifuged for 5 min (12,600 rpm, 7,000 *g;* model 59; Fisher Scientific Co., Pittsburgh, PA) and loaded on 2–12% polyacrylamide gradient SDS gels (cf. Somerville and Wang, 1981). Gels were stained for 3.5 min using an ammoniacal silver stain (cf. Granzier and Wang, 1993*a*). The gels were photographed using Kodak Tech-Pan film and HC-110 developer.

Quantitative densitometry was done with a video densitometer (model 620; Bio-Rad Laboratories, Richmond, CA) with a 100-mm lens (resolution 130 μm). Three scans (50 μm wide) 1 mm apart were averaged for each lane. Peak areas were determined using 1-D Analyst II software (Bio-Rad Laboratories) (cf. Granzier and Wang, 1992). Peak areas were normalized to paramyosin, which serves as an internal control for the variation of fiber size.

General Protocol

Single fibers (1.5–2 mm long) in relaxing solution D were first twisted by 180° and mounted to the force transducer and servomotor such that the fibers were slightly shorter than their slack length. The minor and major fiber diameters (typically 20–30 μm) were measured with a ×40 objective lens and a calibrated ×10 ocular. Cross-sectional area was calculated assuming an elliptical cross-section. The fibers were then removed, untwisted, and remounted. To ensure a stable slack length throughout the mechanical protocol, the fiber and the clip-hook attachments were first exposed several times to the high forces that fibers generate in rigor solution. The fiber was then kept in relaxing solution for 10 min while the fiber was made to buckle slightly by moving the translators. Slack length was determined by slowly moving the translators and finding the distinct length at which the fiber was just straight and did not yet develop passive force. Next, the sarcomere length detector was calibrated and the sarcomere length of the central region of the fiber was followed throughout the experiment.

Mechanical properties of the fibers were characterized before and after gelsolin treatment using identical protocols. After the mechanical experiment, the fiber was removed from the chamber, solubilized, and electrophoresed for protein analysis. Blank coupling for the frequency sweep protocol was measured after each experiment under conditions identical to those of the experiment. Experiments were carried out at room temperature (21–23°C).

In the study of the effect of ionic strength on passive stiffness, fibers were equilibrated for 20

min each in relaxing solutions from high to low ionic strength (for composition see Table I) before stiffness was measured. To rule out irreversible changes, the fiber was returned to the μ = 130 mM solution (solution D) repeatedly and mechanical properties were measured. All fibers in this study produced consistent control curves throughout the entire experiment.

Definitions

Stiffness	Complex stiffness measured at 2.2 kHz with the constant frequency protocol using a 0.1% amplitude unless otherwise stated
Passive (resting or nonactivated) fiber	Skinned fiber present in relaxing solution (D) containing 5 mM MgATP and pCa >9.0
Active tension/stiffness	The difference between total tension/stiffness of fiber in solution E and passive tension/stiffness of the same fiber in relaxing solution D undergoing the same stretch-release protocol and an identical period of stress relaxation (see Fig. 3 *A*)
Rigor tension/stiffness	The difference between total tension/stiffness of fiber in solution F and passive tension/stiffness of the same fiber in relaxing solution D undergoing the same stretch-release protocol and an identical period of stress relaxation (see Fig. 3 *A*)
Yield point	The degree of sarcomere extension at the elastic limit (see Fig. 4 *B*)
Pre-yield fibers	Fibers that have not been subjected to stretch beyond the yield point
Postyield fibers	Fibers that have been subjected to stretch beyond the yield point
Weak-binding cross-bridge (weak bridge)	Low actin affinity cross-bridge with rapid kinetics that produces no tension
Strong-binding cross-bridge (strong bridge)	High actin affinity cross-bridge with slower kinetics that does produce tension

RESULTS

Pilot Experiments

Most results reported in this study were obtained from fresh fibers. When live bugs were not available, glycerinated fibers were used (as indicated in figure legends). A comparative study indicated that the mechanical characteristics of fresh and glycerinated fibers (prepared as described in Materials and Methods) were similar and no statistically significant (P = 0.05) differences were found in, for example, the slope of the passive tension-length relation, the maximum passive tension, the degree of sarcomere extension at maximum tension, and the stiffness and phases measured at a wide range of frequencies by the frequency sweep protocol (results not shown).

Typical passive tension-sarcomere length curves are shown in Fig. 2 *B*. Passive tension rose steeply with sarcomere length and reached a maximal value at the yield point when the fiber was stretched by 6–7% of the slack length (loop 2 of Fig. 2 *B*).

Stretching insect fibers beyond the yield point resulted in slight decline (~20% in loop 2) in tension. Upon total release, the fiber returned to a new slack length that was significantly longer (2.88 μm) than the original value (2.76 μm). Subsequent tension-length loops (3 and 4) had reduced slopes, with a further increase of slack length (2.99 μm). Such alterations were absent when fibers were cycled below the yield point (loop 1). To avoid undesirable alterations of mechanical characteristics of overstretched fibers, we investigated only pre–yield point fibers. This was achieved by limiting total fiber stretch to maximally 5% of slack length, and limiting stretch rates to maximally 0.05% per s. Furthermore, at the completion of each stretch-release cycle, a rest period of at least 20 min was imposed at slack length. Otherwise, tension-length loops were not reproducible. In this fashion, superimposable tension-length loops were obtained when the fiber was subjected to many stretch-release cycles (>20) for a period of a least 10 h at room temperature.

Thin Filament Removal by Gelsolin Treatment

When gelsolin was added to fibers in rigor, both tension and stiffness decreased by ~90% within 10 min of incubation with a half-time of 2 min, while sarcomere length increased to the value measured before rigor induction (Fig. 5). After a second gelsolin treatment of 5 min in activating solution and the removal of fragmented thin filaments in relaxing solution, the mechanical properties of the fiber were measured and the degree and the site of actin removal by gelsolin was subsequently monitored by SDS gel electrophoresis and fluorescent staining of actin.

Gel electrophoresis showed that gelsolin treatment extracted actin, arthrin, troponin-T, troponin-H, and tropomyosin. Quantitative densitometry indicated that these proteins were removed to the extent of 82–93% (Fig. 6). In particular, actin was reduced by 84% of its control value.

To locate the site of actin removal, myofibrils were stained with rhodamine-phalloidin, which binds F-actin. In untreated controls, phalloidin labeled the whole sarcomere more or less uniformly except for a narrow clear zone in the center (H zone) and a more intense zone at the Z line region (Fig. 7, control). Gelsolin treatment removed phase density in the overlap region without obvious effect on the Z line (Fig. 7, phase). Phalloidin staining of the gelsolin-treated myofibrils showed that actin outside the Z line region of the sarcomere was removed, while actin in the Z line remained unextracted (Fig. 7, treated). Increasing extraction time in activating solution from 5 to 30 min caused no further change in staining patterns. Z line actin thus resists gelsolin extraction. The fraction of total sarcomeric actin that is localized in the Z line can be estimated as 12% (assuming a Z line thickness of 0.125 μm [Squire, 1981], a thin filament length of 1.05 μm [White and Thorson, 1973], and double overlap of thin filaments in the Z line [Ashhurst, 1977]). This value is in general agreement with the 16% value of residual actin estimated by gel electrophoresis, supporting the conclusion that gelsolin treatment has nearly completely removed thin filament actin and associated proteins outside the Z line region.

Tension and Stiffness before and after Gelsolin Treatment

Active tension and stiffness were studied using the constant frequency protocol. Fibers were activated briefly (solution E, Table I) and relaxed again (solution D) each

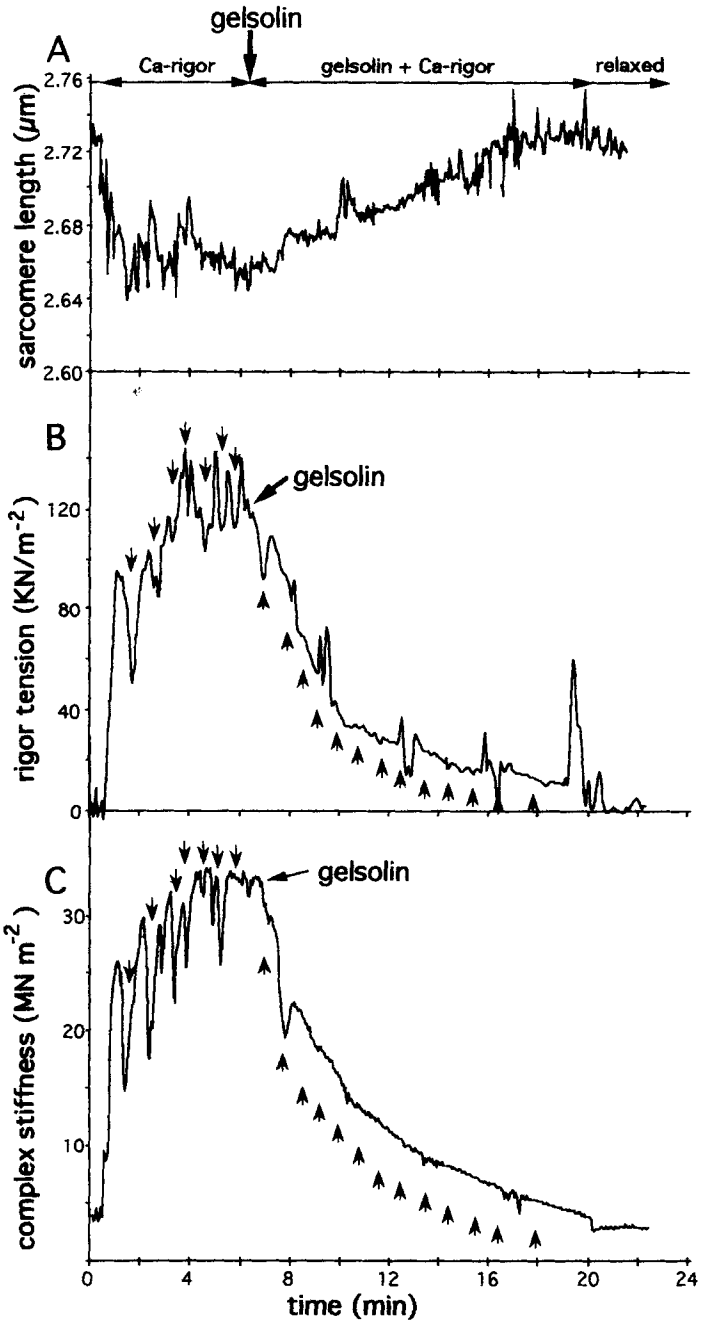

FIGURE 5. Effect of gelsolin treatment on rigor tension and rigor stiffness of a fresh fiber. The fiber was prestretched by 2.5% in relaxing solution. Ca-rigor solution (see Materials and Methods) was then added to the chamber and when tension, stiffness, and sarcomere shortening reached maximal values, gelsolin was added. In response, tension, stiffness, and sarcomere length rapidly returned to baseline values. During gelsolin treatment the solution was mixed by withdrawing and quickly reinjecting 10 μl of solution (upward arrows). The fluctuations in the initial parts of the tension and stiffness traces resulted from disturbances while injecting rigor solution into the chamber (downward arrows).

time before a new step or release was imposed. Before gelsolin treatment (Fig. 8, top left panel; Table II), active tension was very low at short length ($\sim$5 kN m^{-2} at 1% prestretch) and increased greatly with increasing lengths (72 kN m^{-2} at 5% stretch). When fibers were subsequently released, active tension decreased to levels that were significantly less than those after stretch to the same length; i.e., the active

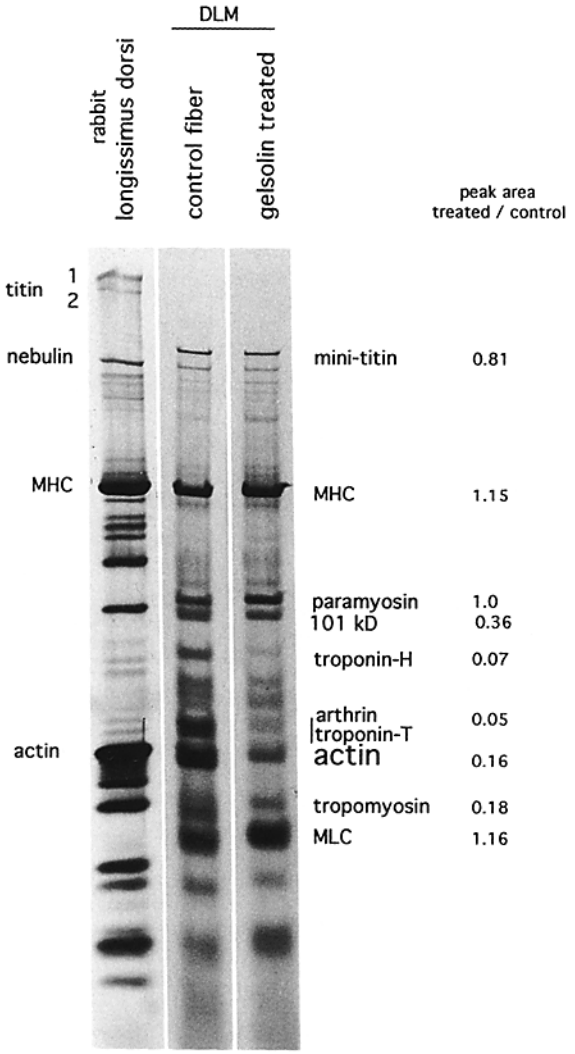

FIGURE 6. Effect of gelsolin treatment on gel patterns. Short segments of treated fresh fibers were solubilized at 60°C and loaded on a 2–12% gradient polyacrylamide gel. As controls, 500 ng of solubilized rabbit Longissimus dorsi myofibrils and an untreated *Lethocerus* DLM fiber were electrophoresed on the same gel. The gel was silver-stained for 3.5 min and peak areas were determined using video densitometry and normalized to paramyosin to facilitate comparison. Peak areas of troponin-H, arthrin/troponin-T (unresolved), actin, and tropomyosin are greatly reduced in the treated fiber. Minititin suffered a 19% loss during the treatment, while passive tension of this fiber was reduced by 12%. (The 101-kD band consists of a doublet in higher resolution gels. Only the upper band was extracted by gelsolin (Granzier and Wang, 1993*b*).

tension–sarcomere length relation showed hysteresis (Fig. 8, top left panel). For example, at 4% extension active tension was only 25 kN m^{-2} after release and 60 kN m^{-2} after stretch (Fig. 8, top left panel).

It is unlikely that hysteresis results from errors in sarcomere length measurement, since the difference in sarcomere length at a given tension amounts to 20–40

nm/sarcomere (Fig. 8, top left panel), which is substantially larger than the experimental errors in sarcomere measurement (<5 nm/sarcomere). Since sarcomere extension from the slack length results in a decrease of overlap between thin and thick filaments (slack length fibers have H zones; unpublished data), neither the increase in active tension nor the hysteresis phenomenon can be understood solely on the basis of the extent of filament overlap. In searching for a correlation, it was found that active tension is closely correlated to passive tension measured just before activation. As seen in Fig. 9 *A*, plots of active tension vs. passive tension revealed a biphasic behavior: for passive tension <5–10 kN m^{-2}, active tension remained close to zero; above this threshold, active tension increased linearly with passive tension. Furthermore, the relation was free of hysteresis. Active stiffness varied with passive tension in a way similar to active tension (Fig. 9 *A*), while active stiffness was linearly related to active tension (Fig. 9 *B*). The striking correlation between passive and

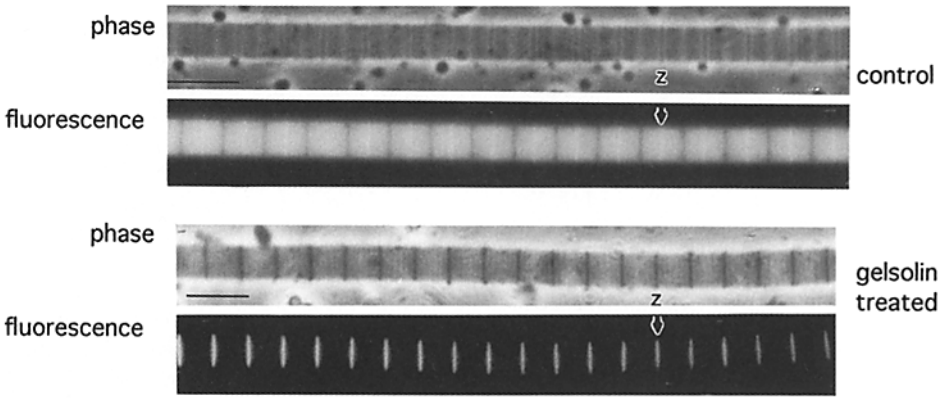

FIGURE 7. Specific removal of thin filament by gelsolin. Myofibrils before and after gelsolin treatment were labeled with rhodamine-phalloidin to stain F-actin. In the untreated controls, actin staining was found in the whole sarcomere except for a narrow zone in the center (H zone), with the most intense staining at the Z line region. After gelsolin treatment only Z line staining remained. Scale bar, 5 μm.

active tension suggests that active tension in waterbug flight muscle is regulated by the passive tension level.

After gelsolin treatment, active tension had decreased by >95% at all lengths (Fig. 8, top left panel), with a similar decrease in active stiffness (Fig. 8, top right panel). Since it is well established that active tension and stiffness arise from actomyosin interaction, these mechanical data confirmed the quantitative removal of thin filaments by gelsolin treatment.

Rigor tension and rigor stiffness were very high before gelsolin treatment, and both tension and stiffness increased slightly with sarcomere length (Fig. 8, middle panels). It is interesting that the tension-stiffness ratio during rigor ($4.5 \pm 0.16 \times 10^{-3}$; $n = 11$) is much less than the value during activation ($11.53 \pm 1.6 \times 10^{-3}$; $n = 11$). If stiffness is a measure of the number of attached cross-bridges, then this finding

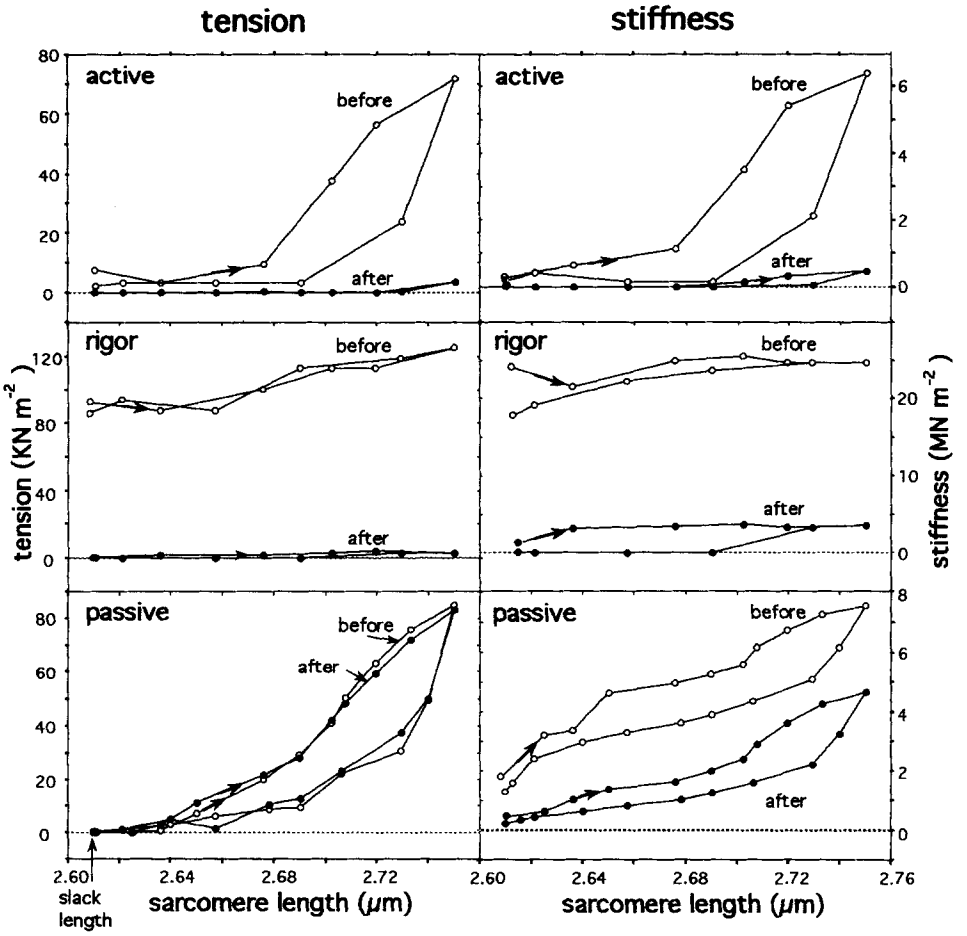

FIGURE 8. Effect of thin filament removal on tension and complex stiffness of a fresh fiber in relaxing, activating, and rigor solutions. The fiber was stretched by 1% with a velocity of 0.01%/s and then held constant for 240 s until the next stretch was imposed. When 5% stretch was reached, the fiber was released with the same velocity as used for stretch. Tension and 2.2-kHz stiffness were determined 220 s after each stretch-release was completed. This constant frequency protocol was repeated three times. In the first cycle, active tension and stiffness (*top panels*) were determined after 180 s of stress-relaxation by activating (solution E) and relaxing (solution D) before the next step-release was imposed (as in Fig. 3). Similarly, by switching to rigor solution (F in Table I), rigor tension and stiffness were determined (*middle panels*). The passive tension and stiffness (*bottom panels*) were determined in the last cycle (solution D in Table I). After these three cycles, the fiber was treated with gelsolin and the three cycles were repeated (indicated in the panels as "after"). Note the difference in scale of the top, middle, and bottom panels.

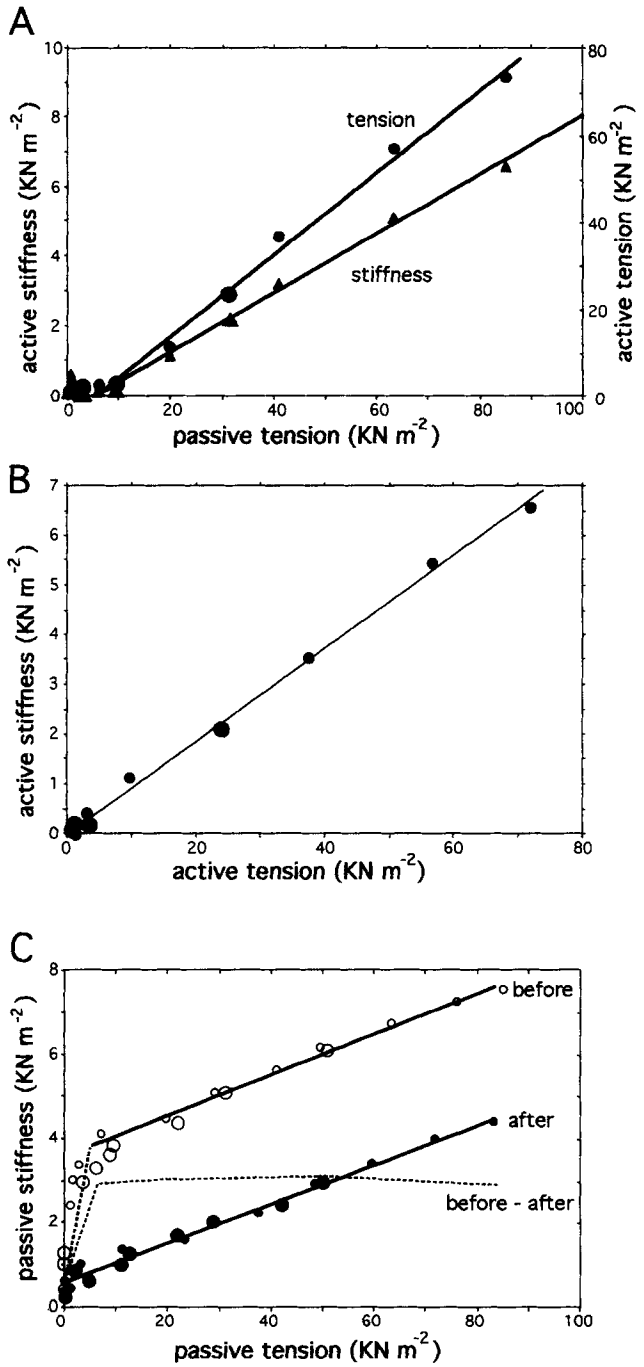

FIGURE 9. Correlation between tension and stiffness of active and passive fresh fiber. (*A*) Active tension vs. passive tension and active stiffness vs. passive tension. (*B*) Active stiffness vs. active tension relation. (*C*) Passive stiffness vs. passive tension relation. Data are from Fig. 8. *Small symbols,* stretch curve; *large symbols,* release curve. The straight lines in *A* and *B* are regression lines obtained by fitting data with passive tension higher than 10 kN m^{-2} (See Discussion). Linear regression lines in *A:* active tension, $y = 0.95x - 5.5$; $r^2 = 0.99$; active stiffness, $y = 0.085x - 0.43$; $r^2 = 0.99$; in B: $y = 0.094x - 0.029$; $r^2 = 0.99$. This line passed through the origin of the axis (95% confidence level). Lines in *C* before gelsolin treatment (before); $y = 0.047x + 3.67$; $r^2 = 0.97$; after treatment (after): $y = 0.049x + 0.6$; $r^2 = 0.98$.

implies that the average attached cross-bridge generates much less force during rigor than during activation.

After gelsolin treatment, rigor tension (Fig. 8, middle left panel) had decreased 98 ± 0.5% (n = 11). Rigor stiffness (Fig. 8, middle right panel), on the other hand, had decreased by 87 ± 1.6% (n = 11), significantly less than the decrease in rigor tension. It appears that part of total rigor stiffness is independent of the thin filaments.

TABLE II

Effect of Gelsolin Treatment on Passive, Active, and Rigor Properties

Tension measurements*

Stretch (%)	Passive tension (kN m^{-2})		Active tension (kN m^{-2})		Rigor tension (kN m^{-2})	
	Before	After (% of before)	Before	After (% of before)	Before	After (% of before)
1	8.47 ± 2.9	97 ± 8	5.3 ± 7.1	19 ± 14	75.1 ± 21.7	9 ± 8
2	15.4 ± 3.7	99 ± 29	21.2 ± 21.0	15 ± 20	81.3 ± 20.5	11 ± 6
3	27.3 ± 8.7	99 ± 30	35.4 ± 15.9	12 ± 16	81.7 ± 21.5	13 ± 7
4	39.1 ± 14	97 ± 6	59.5 ± 16.1	7 ± 6	85.1 ± 23.0	13 ± 8
5	51.5 ± 19.4	98 ± 10	72.2 ± 16.0	12 ± 6	90.0 ± 27.0	10 ± 6

Dynamic measurements on passive fibers‡

Frequency (Hz)	Complex stiffness (MN m^{-2})		Phase shift (deg)	
	Before	After (% of before)	Before	After
0.025	4.0 ± 1.2	83 ± 7	7.8 ± 3.0	4.0 ± 5.6
0.25	3.7 ± 1.2	79 ± 11	2.5 ± 1.7	2.5 ± 0.7
2.5	3.8 ± 1.3	81 ± 11	−0.1 ± 1.4	−0.2 ± 1.9
25	4.0 ± 1.3	78 ± 11	0.2 ± 1.0	0.2 ± 0.4
100	4.1 ± 1.3	73 ± 10	3.8 ± 1.8	0.6 ± 2.1
250	4.2 ± 1.2	72 ± 10	7.2 ± 4.7	2.7 ± 1.6
1,000	5.5 ± 0.9	65 ± 11	17 ± 7.2	6.2 ± 5.1
2,500	7.9 ± 2.5	54 ± 6	14 ± 3.3	4.3 ± 3.8

*Same protocol as described in legend of Fig. 5. The values are the mean and SD of typically five fibers (range two to six).

‡The fibers were prestretched by 2.5% (velocity 0.025%/s). 200 s after completing the stretch sinusoidal length perturbations were imposed (amplitude 0.1%) at frequencies from 0.025 to 2,500 Hz. The complex stiffness and the phase shift between length and tension were determined. The values are the mean and SD of four fibers.

Passive tension was affected very little by gelsolin treatment: while there was a slight decrease in some experiments, a slight increase was observed in others (range −15 to +7%). Overall the tension-length loops were very similar before and after treatment (Fig. 8, bottom left panel; Table II). In contrast, passive stiffness (2.2 kHz) was reduced by ~50% (Fig. 8, bottom right panel). Plots of passive stiffness vs. passive tension for fibers before and after treatment were both linear and parallel to each other above 5–10 kN m^{-2} of passive tension (Fig. 9 *C*). Interestingly, the net reduction of passive stiffness by gelsolin was independent of passive tension (Fig. 9 *C*, before − after).

Further studies with the frequency sweep protocol showed that after gelsolin treatment both passive stiffness and phase were depressed over the whole frequency range (0.2–2,500 Hz) and that the depression increased with frequency (Fig. 10, *A* and *B;* Table II). Particularly striking was the abolishment of the steep increase of untreated fibers in stiffness and phase at frequencies higher than 250 Hz. A plot of viscous moduli vs. elastic moduli (Fig. 10 *C*) indicated that gelsolin treatment effectively removed the viscous component of the complex stiffness at frequencies higher than 250 Hz.

Effect of Ionic Strength on Passive Tension and Stiffness

An obvious candidate for the portion of passive high frequency stiffness that is abolished by thin filament removal is actomyosin interaction (weak-binding cross-bridges). The kinetics of weak bridges are highly sensitive to ionic strength and the weak bridge stiffness of relaxed rabbit fibers increases greatly with decreasing ionic strength (Schoenberg, 1988). To explore the presence of actomyosin interaction in relaxed insect flight muscle, we studied the ionic strength sensitivity of passive high frequency stiffness before and after thin filament removal.

Very little effect of ionic strength on passive tension was observed. Tension-length loops at the various ionic strengths were superimposable during both stretch and release (Fig. 11 *A*). In contrast, passive stiffness was sensitive to ionic strength and decreased about twofold during both stretch and release when μ was increased from 45 to 195 mM (Fig. 11 *B*). The difference between complex stiffness measured at 45 and 195 mM (ΔE) increased from 2.67 μm (slack length) to 2.72 μm and dropped slightly thereafter.

Plots of passive stiffness vs. passive tension were superimposable for both stretch and release (Fig. 11 *C*, small and large symbols). These plots are linear (Fig. 11 *C*) except for data points with very low tension (see Discussion). Interestingly, these lines had similar positive slopes at the different ionic strengths but were shifted along the stiffness axis (Fig. 11 *C*); i.e., the differences between the stiffness values at the three ionic strengths did not vary with passive tension.

Effect of Ionic Strength after Gelsolin Treatment

After gelsolin treatment, ionic strength had no significant effect on passive tension at any degree of stretch or release (Fig. 12 *A*). High frequency stiffness, on the other hand, was diminished by actin extraction at all ionic strengths; the decrease was largest at 45 mM, intermediate at 130 mM, and smallest at 195 mM (Fig. 12 *B*). It is interesting that stiffness-length loops of thin filament-free fibers at the different ionic strengths are nearly superimposable (Fig. 12 *B*). Additionally, hysteresis is similar in magnitude at the three ionic strengths before and after thin filament removal (Fig. 12 *B*).

After thin filament removal, plots of passive stiffness against passive tension showed superimposable linear curves at the three ionic strengths (Fig. 12 *C*). Before gelsolin treatment, the stiffness-tension relation at μ = 45 mM is biphasic and can be fitted by either of two straight lines, as in Fig. 12 *C*, or by a hyperbolic curve with transition to saturation near 10 kN m^{-2} of passive tension (not shown). The biphasic nature is less pronounced but still detectable at 130 and 195 mM, and is abolished or

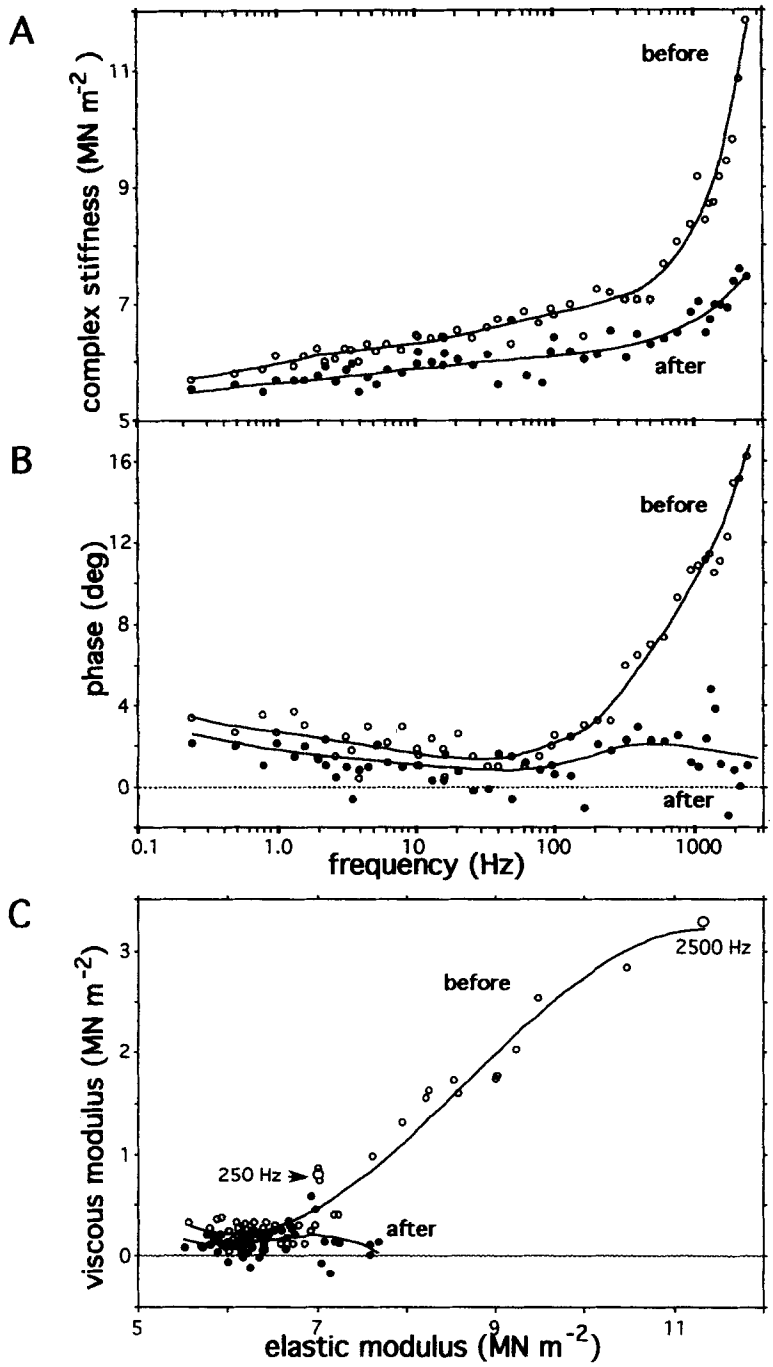

FIGURE 10. Effect of thin filament removal on frequency dependence of stiffness and phase of passive fresh fiber. The frequency sweep protocol was imposed with a stretch amplitude of 4.5% and stretch velocity of 0.045%/s and a frequency sweep was imposed 240 s after completion of stretch. Both complex stiffness (*A*) and phase angle (*B*) were depressed after gelsolin treatment, especially at high frequencies. Nyquist loops in *C* show that the viscous moduli at frequencies >250 Hz are greatly depressed by gelsolin treatment. Curves are fifth-order polynomial fits.

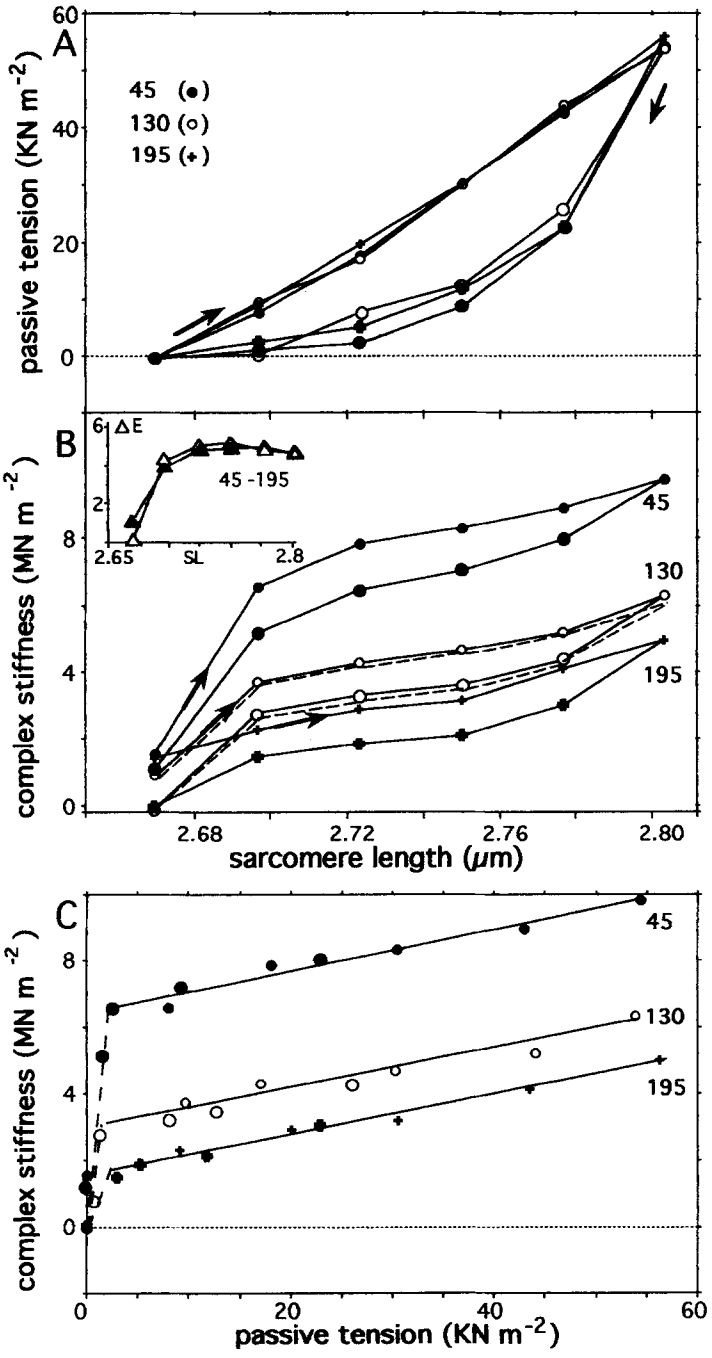
A
45 (●)
130 (○)
195 (+)
passive tension (KN m^{-2})
60
40
20
0
B
ΔE
45 -195
6
2
2.65
SL
2.8
45
130
195
complex stiffness (MN m^{-2})
8
4
0
2.68
2.72
2.76
2.80
sarcomere length (μm)
C
45
130
195
complex stiffness (MN m^{-2})
8
4
0
0
20
40
60
passive tension (KN m^{-2})

FIGURE 11

greatly diminished by gelsolin treatment. It is striking that the slopes of the passive stiffness-tension relation are similar before and after thin filament removal (Fig. 12 *C*).

The frequency sweep protocol showed that after thin filament removal, stiffness varied little with frequency and that stiffness-frequency curves were nearly superimposable at the three ionic strengths (Fig. 12 *D*).

DISCUSSION

Functional Dissection of Mechanical Properties of Insect Flight Muscle

The selective removal of thin filaments by gelsolin, a technique introduced by Funatsu et al. (1990) for structural studies of elastic filaments in vertebrate skeletal muscle, proves to be a powerful technique to investigate the mechanics of insect flight muscle in active, passive, and relaxed states. Since gelsolin only removes actin and associated proteins (Figs. 6 and 7), we have been able to study for the first time the intrinsic mechanical properties of C filaments. The observation that the passive tension–sarcomere length relation was not affected by thin filament removal indicates that passive tension is solely a mechanical manifestation of the C filament in response to sarcomere stretch. Passive stiffness, however, consists of two components. The component that is sensitive to ionic strength and is eliminated by gelsolin treatment requires the participation of actin and can be attributed to actomyosin interaction (weak bridges) in passive muscle. The other passive stiffness component that remains after gelsolin treatment is probably a sole property of the C filament. Similar analysis of gelsolin sensitivity of active tension and active stiffness shows that they are derived from force-generating strong bridges, as expected (see below). Analysis of rigor muscle, however, indicates that while rigor tension is entirely actin based, rigor stiffness contains a component that resists gelsolin treatment and is therefore probably C filament based.

The successful dissection of the mechanical properties and the assignment of their

---

Figure 11 (*opposite*). Effect of ionic strength on passive tension and passive stiffness of a glycerinated fiber. The ionic strength was altered by sequentially replacing solution in the chamber with relaxing solutions of decreasing ionic strength (195, 130, and 45 mM). The fiber was then returned to 130 mM to confirm reproducibility. The fiber was stretched by 1% with a velocity of 0.01%/s and then held constant for 80 s until the next stretch was imposed. When 5% total stretch was reached, the fiber was released in steps with the same velocity as that used during stretch. Tension and stiffness values at the end of the 80-s period are plotted in *A* and *B*. Inset in *B* shows the difference between complex stiffness measured at μ = 45 and μ = 195 mM (ΔE, complex stiffness in MN m^{-2}; SL, sarcomere length in μm). The broken line in *B* indicates the result obtained with solution G + 85 mM K-propionate; the solid line was obtained with solution D. In *C*, passive stiffness is plotted against passive tension (data from *A* and *B*). The linear lines are regression lines of data points with passive tension > 10 kN m^{-2}. The slopes of the solid linear regression lines are: 0.062, 0.056, and 0.058 at μ = 45, 130, and 195 mM, respectively. The *y*-intercepts are 6.5, 3.1, and 1.63 (MN m^{-2}), in the same order. Data points during stretch and release are differentiated with small symbols and large symbols (*A–C*), respectively, and with open and closed symbols (*B, inset*).

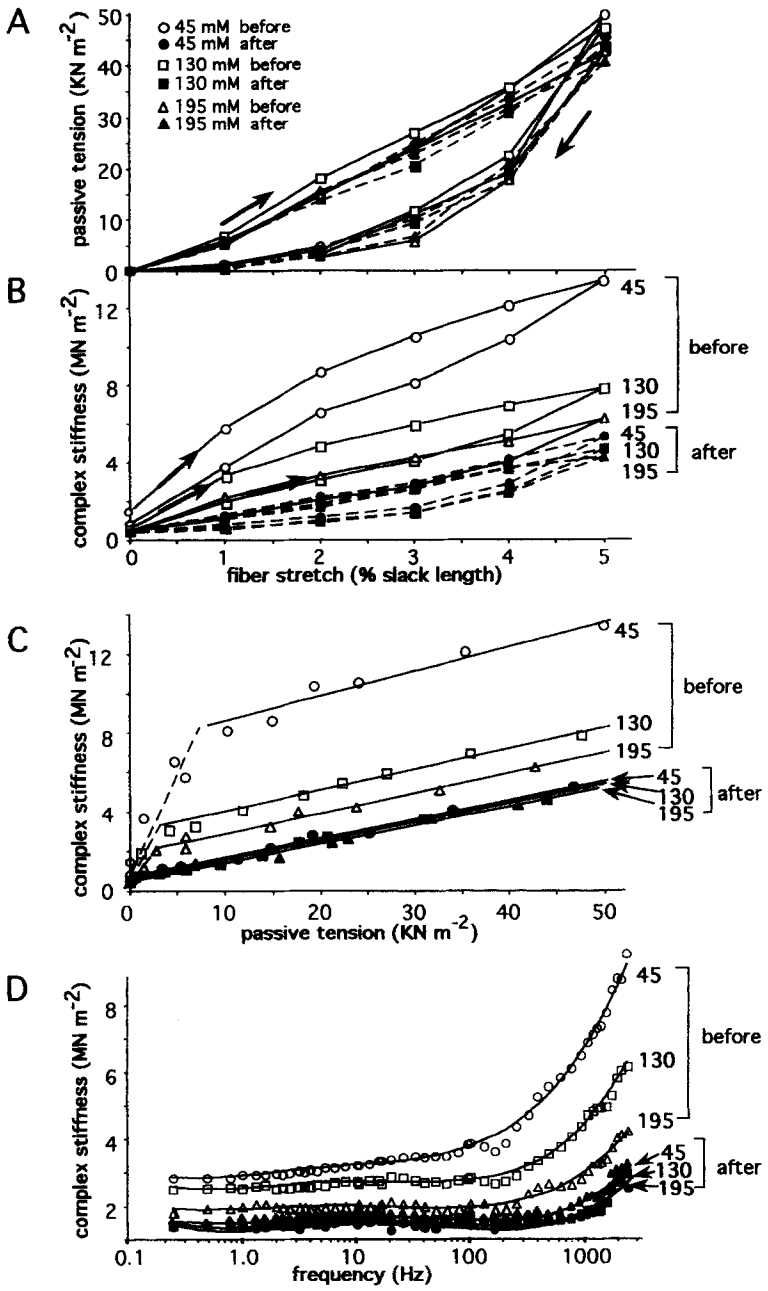
A
B
C
D
45 mM before
45 mM after
130 mM before
130 mM after
195 mM before
195 mM after
passive tension (KN m-2)
complex stiffness (MN m-2)
fiber stretch (% slack length)
before
after
45
130
195
passive tension (KN m-2)
frequency (Hz)

FIGURE 12

structural basis now provides a foundation for further analysis and investigation of their interplay.

Passive Tension and Segmental Extension of C Filaments

Passive tension of insect flight muscle increases steeply with sarcomere length between 0 and 5% stretch and reaches a yield point at >6–7% stretch (Fig. 2 *B*). In contrast, the passive tension of rabbit skeletal muscle is very low between 0 and 40% sarcomere stretch and increases exponentially until a yield point is reached at 70–100% sarcomere extension (Wang et al., 1991).

Our recent analysis of passive tension-sarcomere length curves of vertebrate muscles (Wang et al., 1991, 1993)[1] have identified several parameters that underlie these curves: (*a*) the slack length and degree of stretch of an extensible titin segment localized between the Z line and the end of the thick filament; (*b*) the intrinsic force-generating capacity of titin; (*c*) the strength of the titin–thick filament connection. It was concluded that a yield point occurs when the passive tension of the extensible titin segment is high enough to dislodge the titin–thick filament connection near the end of the thick filaments, thereby recruiting anchored titin into the extensible pool. Thus, the reduction in the slope of the tension–length curve of postyield fibers is likely to result from the net increase of the extensible titin segment. Our present data on insect flight muscle provide an opportunity to test the segmental extension concept on tension–length curves that are quantitatively different from those of vertebrate muscle (Fig. 13).

Each C filament is thought to consist of two distinct segments (I and A segments). Below the yield point only the I segment is extensible and involved in passive tension development, while the A segment is extensible. Above the yield point, the A segment is partially released from physical constraints and becomes extensible. We assumed that the I segment length of the C filament is equal, or proportional, to the I band width. For slack sarcomeres (no passive tension), I band width was taken as 0.05 μm (White, 1983), and the I band extension during stretch was taken as half of the increase in sarcomere length. Furthermore, in postyield sarcomeres the net increase in sarcomere length of slack fibers was assumed to be the result of an increase of I band width. Therefore, the slack I segment length had increased accordingly (0.11 μm in loop 3 of Fig. 2 *B;* 0.17 μm in loop 4).

When tension is plotted against I segment strain for all four loops shown in Fig.

Figure 12 (*opposite*). Effect of thin filament removal and ionic strength on passive tension and passive stiffness of a fresh fiber. The fiber was subjected to the same protocols and solution exchanges as in Fig. 11, both before and after gelsolin treatment. (*A–C*) Constant frequency protocol; (*D*) frequency-sweep protocol. Thin filament removal caused little change in passive tension (*A*), yet significantly reduced passive stiffness at all ionic strengths (*B*). The straight lines in *C* are linear regression lines of data with passive tension >10 kN m^{-2}. Slopes of the lines before actin removal: 0.106, 0.110, and 0.108 at μ = 45, 130, and 195 mM; after actin removal (in same order): 0.104, 0.098, and 0.097. The extrapolated *y*-intercepts (in MN m^{-2}) differed before actin removal (8.22, 2.82, and 1.82) but were similar after actin removal (0.72, 0.71, and 0.65). (*D*) Complex stiffness–frequency relation. Thin filament removal resulted in a reduction of stiffness at all frequencies and rendered stiffness insensitive to ionic strength at all frequencies.

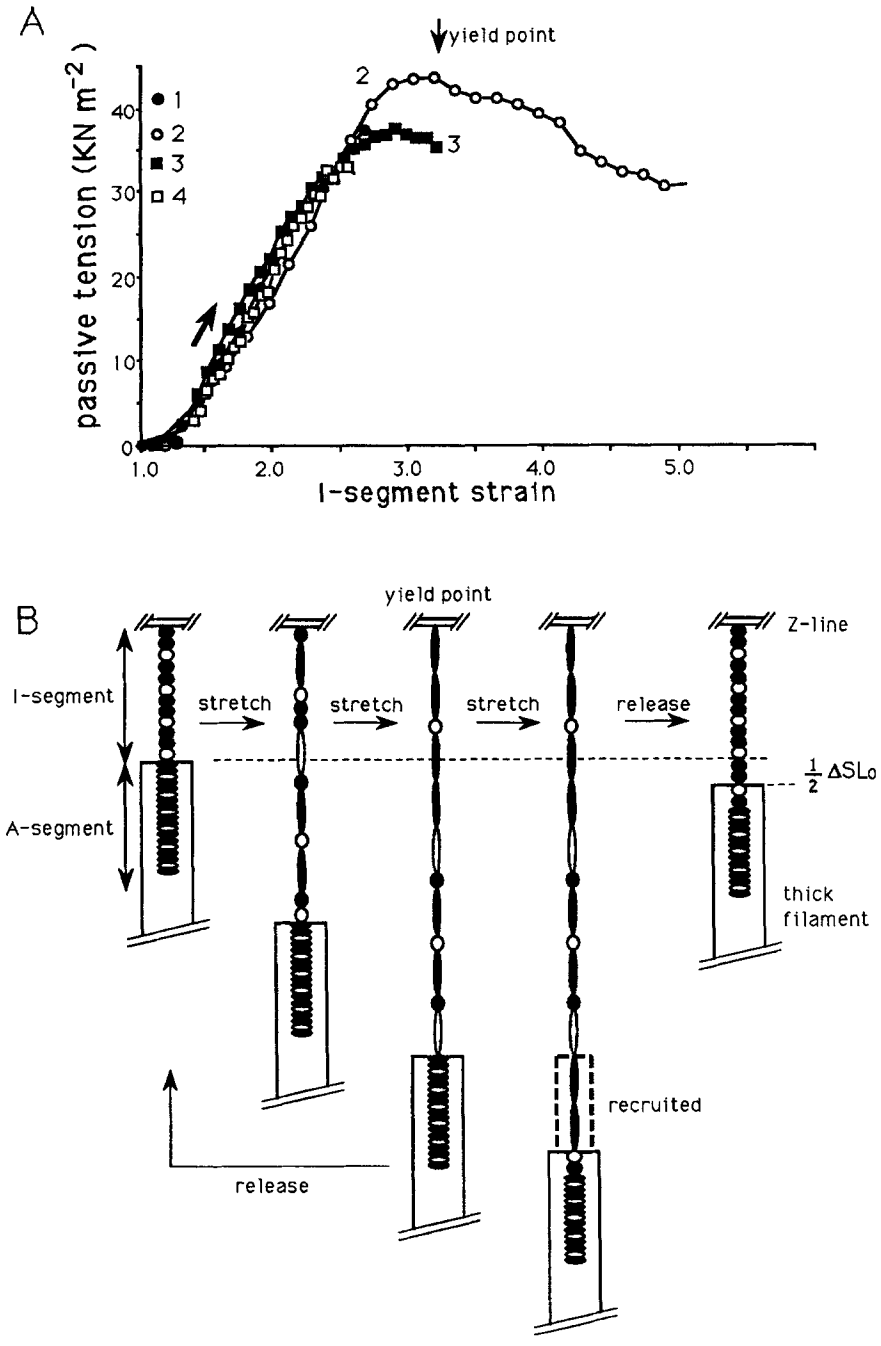
A
yield point
2
1
2
3
4
3
passive tension (KN m^{-2})
40
30
20
10
0
1.0
2.0
3.0
4.0
5.0
l-segment strain
B
yield point
Z-line
l-segment
stretch
stretch
stretch
release
$\frac{1}{2}\Delta SL_0$
A-segment
thick
filament
recruited
release

FIGURE 13

2 *B*, stretch curves of both preyield fibers (loops 1 and 2) and postyield fibers (loops 3 and 4) are superimposable (Fig. 13 *A*). These results suggest that the segmental extension model of passive tension development based on work with vertebrate muscle is equally applicable to insect flight muscle. It is also striking that despite significant differences in sarcomere structure and molecular make-up of vertebrate muscle and insect flight muscle, the yield point occurs in insect and vertebrate muscle at a similar segmental strain of ~3.5.

Passive stiffness of the C filament increases linearly with passive tension (Fig. 9 *C;* bottom lines of Fig. 12 *C*). This relation differs from that of a simple Hookean spring and may reflect the mechanical response of a gel-like lattice of C filaments (Pringle, 1977), or it might be intrinsic to the C filament itself. It is tempting to speculate that the dual sequence motif structure of minititin (Benian et al., 1989; Ayme-Southgate, 1991) may contribute to the linear stiffness–tension relation. If the two types of motifs of minititin display different stiffness, then a linear combination of such motifs is, theoretically, able to have a composite tension–stiffness relation that is linear (Granzier, H., and K. Wang, unpublished results).

Active Tension

When insect flight muscle is activated, a long-lasting contraction with a constant level of tension develops (Fig. 3 *A*). However, we found that high levels of active tension are obtained only when there is a high level of passive tension before activation (Fig. 9 *A*). Passive tension in turn is determined by the degree of sarcomere extension, the rate of stretch, the duration of passive stress relaxation, the direction of length change (stretch vs. release), and whether the fiber has been stretched to exceed the elastic limit at the yield point (preyield vs. postyield fibers). This striking relation between active and passive tension points to a potentionally important mechanical interaction between the proteins that generate active tension (myosin) and those that bear passive tension (minititin). From an experimental view point, this relation could explain why it was difficult in our earlier attempts to reproducibly generate the same level of active tension by controlling the fiber length alone. It might also explain at least some of the variation in isometric tension and the level of stretch activation reported by others (e.g., Yamakawa and Goldman, 1991).

Figure 13 (*opposite*). (*A*) Passive tension–I segment strain relation. I segment length is estimated as the distance between the end of the thick filament and the Z line, and strain is expressed as a length ratio. Passive tension curves during stretch of the four cycles of Fig. 3 *B* are nearly superimposable. See Discussion for further details. (*B*) Segmental extension model for passive tension generation. The C filament consists of a long string of modules that make up an I and an A segment. Below the yield point only the I segment is extensible and develops passive tension, while the A segment is inextensible. When sarcomere stretch exceeds the yield point, part of the A segment is recruited into the I segment and becomes elastic, and as a result I segment strain and passive tension remain constant. In this model, A segment modules before recruitment are compressed, and compression is permanently relieved after recruitment. This results in an increase of both I band width and sarcomere length at the slack length. Also note that the C filament is depicted as containing two types of mechanical units (open and closed) with different stiffness. See Discussion for further details.

The maximal active isometric tension at 5% prestretch is 72 kN m^{-2} (Table II). This value is about half of the maximal tension generated by vertebrate skeletal muscles at a similar temperature (e.g., Granzier, Wiersma, Akster, and Osse, 1983). Insect flight muscle can be estimated to contain twice as many myosin molecules per thick filament as found in vertebrate thick filaments (White and Thorson, 1973; Goody, Reedy, Hofmann, Holmes, and Reedy, 1985; Squire, 1986), while the number of thick filaments per unit cross-sectional fiber area is ~25% less (Pringle, 1965; White and Thorson, 1973). Taking these differences into account, and assuming that the same fraction of myosin molecules is generating active tension in both tissues, then maximal active tension per myosin molecule of insect and vertebrate muscle are about the same. Thus, insect flight muscle, when prepared and activated properly, can generate active tension per myosin molecule that is comparable to that of vertebrate muscle.

Weak-binding Cross-Bridges: Gelsolin and the Ionic Strength–sensitive Component of Passive Stiffness

The most striking effect of actin removal on passive insect fibers is the large reduction in high frequency stiffness and phase angle (Figs. 8–10 and 12). The stiffness component that is removed is also very sensitive to ionic strength (Figs. 11 and 12). On the other hand, passive tension is affected very little by either thin filament removal or ionic strength variation (Figs. 11 and 12). Before actin removal, plots of passive stiffness vs. passive tension at various ionic strengths can be fitted above 5–10 kN m^{-2} with a family of parallel straight lines with different stiffness intercepts (Fig. 9, bottom panel, and Figs. 11 *C* and 12 *C*). After actin removal, the plots remain linear with similar slopes but greatly reduced stiffness intercepts. Additionally, the relation is no longer sensitive to ionic strength (Fig. 12 *C*). Taken together, our data suggest that the high passive stiffness of insect flight muscle can be resolved into two components: one that varies linearly with passive tension and is insensitive to ionic strength (this component determines the slope) and a second one that is independent of passive tension, varies with ionic strength, and determines the stiffness intercept.

The stiffness component that is sensitive to ionic strength requires the participation of the thin filament since it is abolished after gelsolin treatment (Fig. 12, *C* and *D*). An obvious candidate for this stiffness component is actomyosin interaction that contributes to stiffness but not to tension, i.e., the weak-binding cross-bridge. It is now well accepted that such cross-bridges exist in relaxed rabbit psoas fibers and can be detected mechanically as high frequency stiffness in the presence of MgATP and at low temperature (Brenner et al., 1982, 1991; Schoenberg, 1988). These bridges in relaxed psoas muscle are favored at low ionic strength, with an ~10-fold increase in number for a decrease in ionic strength from 170 to 20 mM (Brenner et al., 1986). Additionally, the number of weak bridges decreases nearly linearly with filament overlap (Brenner et al., 1982).

Weak bridges are thought to be able to attach to actin but fail to go through a force-generating cycle in the absence of calcium. Calcium ions, however, allow their conversion to force-generating, strongly binding cross-bridges. The concept that weak bridges are obligatory precursors of force-generating bridges is supported by

the recent observation that caldesmon, which binds to actin and blocks actomyosin interaction (for review see Sobue and Sellers, 1991), inhibits both the high frequency stiffness derived from the weak bridges and the active force generated by the strong bridges (Brenner et al., 1991; Chalovich, Yu, and Brenner, 1991). The important question of whether a significant number of weak bridges exist under physiological conditions in relaxed rabbit fibers is left open.

Our interpretation that the gelsolin-sensitive component of passive stiffness of insect flight muscle is derived from weak bridges is supported by the following facts: (*a*) the component is enhanced at low ionic strength (Figs. 11 and 12); (*b*) it is sensitive to filament overlap (see below); and (*c*) it is reversibly inhibited by a COOH-terminal caldesmon fragment (Granzier, Lin, Wang, and Wang, 1993). If this interpretation is valid, weak bridges of insect flight muscle are unique in that they can be demonstrated under physiological conditions: 21–23°C and ionic strength as high as 195 mM (Fig. 12).

The number of weak bridges in relaxed muscle can be estimated by comparing the stiffness of passive fibers with fibers in rigor, assuming that attached cross-bridges generate the same stiffness in both conditions (Schoenberg, 1988). The gelsolin-sensitive stiffness component of relaxed muscle at μ = 195 mM is 9% of the gelsolin-sensitive rigor stiffness (Fig. 12 *C*). Decreasing ionic strength from μ = 195 to 45 mM increases stiffness by 29.1 ± 6.5% (n = 7) of the gelsolin-sensitive rigor stiffness (solution F in Table I). The total weak bridge stiffness at 45 mM is thus likely to be 38% of rigor stiffness (a similar value was obtained by analyzing caldesmon-sensitive stiffness; Granzier et al., 1993). Since ~80% of the myosin heads in insect flight muscle are attached to actin in rigor (Goody et al., 1985), ~30 and 15% of the myosin heads in relaxed insect flight muscle are attached to actin at μ = 45 and 130 mM, respectively.

The dependence of weak bridge stiffness on filament overlap is somewhat complex. Within the small sarcomere length range below the elastic limit (0–5%; Fig. 3), the extra stiffness generated by lowering ionic strength from 195 to 45 mM (ΔE in Fig. 11 *B*) is biphasic with sarcomere length: it is small at slack length, rises rapidly to a maximum at 2% stretch, and decreases a few percent with further extension (Fig. 11 *B, inset*). The small reduction is approximately the expected magnitude since thin-thick filament overlap drops only a few percent when sarcomeres are stretched from 2 to 5%.

The rise in weak bridge stiffness from slack length to ~2% stretch is, however, unexpected. We recently found a similar rise in weak bridge–based stiffness in rabbit psoas fibers when sarcomere length was increased from 1.95 to 2.35 μm (Granzier and Wang, 1993*b*), and this phenomenon might be a general characteristic of weak bridges. Perhaps thin filaments in slack sarcomeres are not taut enough to fully transmit the weak bridge stiffness. Alternatively, the number of weak bridges might be low between slack length and small degrees of stretch. This possibility is supported by the passive stiffness vs. passive tension plots of untreated fibers (Figs. 9 *C*, 11 *D*, and 12 *D*). These plots revealed that the number of weak bridges is close to zero if no passive tension is developed, increases steeply with increasing tension, and reaches saturation near 5–10 kN m^{-2} and beyond (Fig. 9 *C*, broken line). It is conceivable that effective attachment of weak bridges requires a certain threshold of passive

tension to be exerted on the thick filament and that no weak bridge is formed in the absence of passive tension.

Interestingly, a passive tension threshold is also found for active stiffness and active tension. Both start to increase linearly with passive tension only after a passive tension threshold is reached (Fig. 9 *A*). Significantly, the magnitude of the threshold is similar to that of the weak bridge (see also Fig. 13). We conclude that an appreciable number of strong bridges is only found under conditions that allow the weak bridge to exist. These findings are consistent with the notion that the weak bridge is an obligatory precursor of the strong bridge (Brenner et al., 1991; Chalovich et al., 1991).

Additional mechanical properties of insect weak bridges can be deduced from our work. Since passive tension does not vary with ionic strength or actin removal (Figs. 11 and 12), the weak bridge does not generate passive tension. Furthermore, the weak bridge contributes to stiffness at both high and low frequencies (Fig. 12 *D*), including physiological loading frequencies (20–40 Hz; Barber and Pringle, 1965), which suggests that the weak bridge may serve a mechanical role as a generator of stiffness, in addition to being a precursor for the force-generating strong bridge.

Stretch Activation and Stress Activation

Stretch activation is a well-known characteristic of indirect flight muscle (Pringle, 1978; Tregear, 1983). This phenomenon has been studied mainly by imposing a small stretch during activation and, after initial transients have disappeared, measuring the increase of maintained tension. Our observation that active tension is very low at slack length and increases significantly after prestretch of relaxed fibers before activation (Fig. 8, top left panel) may well be a manifestation of the same mechanical events that give rise to stretch activation. Since our protocols and observations differ, however, from those of earlier studies of stretch activation, we have termed the phenomenon "stress activation" to emphasize passive stress as crucial factor in correlating with active tension, without necessarily implying a fundamental distinction of molecular mechanisms.

Two major hypotheses have been advanced in explaining stretch activation. In the first, stretch is thought to increase the number of force-generating cross-bridges by increasing the attachment rate constant and/or decreasing the detachment rate constant (Pringle, 1978; White, 1983). This hypothesis requires a stretch sensor that transduces changes in sarcomere length into altered cross-bridge kinetics. Thin filament proteins such as the unusual troponin-H are potential candidates (Bullard, Leonard, Larkins, Butcher, Karlik, and Fyrberg, 1988). A second hypothesis, the match–mismatch model, proposes that stretch increases the probability of cross-bridge attachment to actin due to matching of the helical structure of the actin and myosin filaments (Wray, 1979; Abbott and Cage, 1984). Despite its appeal, this model failed to receive support from a recent detailed analysis of filament lattices (Squire, 1992). This model is also inconsistent with our observation of hysteresis in the active tension–sarcomere length relation (Fig. 8, top left panel) since it would have predicted the same tension at a given sarcomere length.

Assuming that the increase in stiffness measured upon activation (Fig. 3 *A*, bottom trace) is a measure of the number of force-generating cross-bridges, then the finding

that active stiffness increases linearly with active tension (Fig. 9 *B*) supports the notion that the number of force-generating cross-bridges increases with stretch and that this underlies the increase in active tension. Additionally, since both the passive tension–active tension relation and the passive tension–active stiffness relation are hysteresis free (Fig. 9 *A*), it can be concluded that the net number of force-generating bridges is influenced by the magnitude of passive tension (or passive stress).

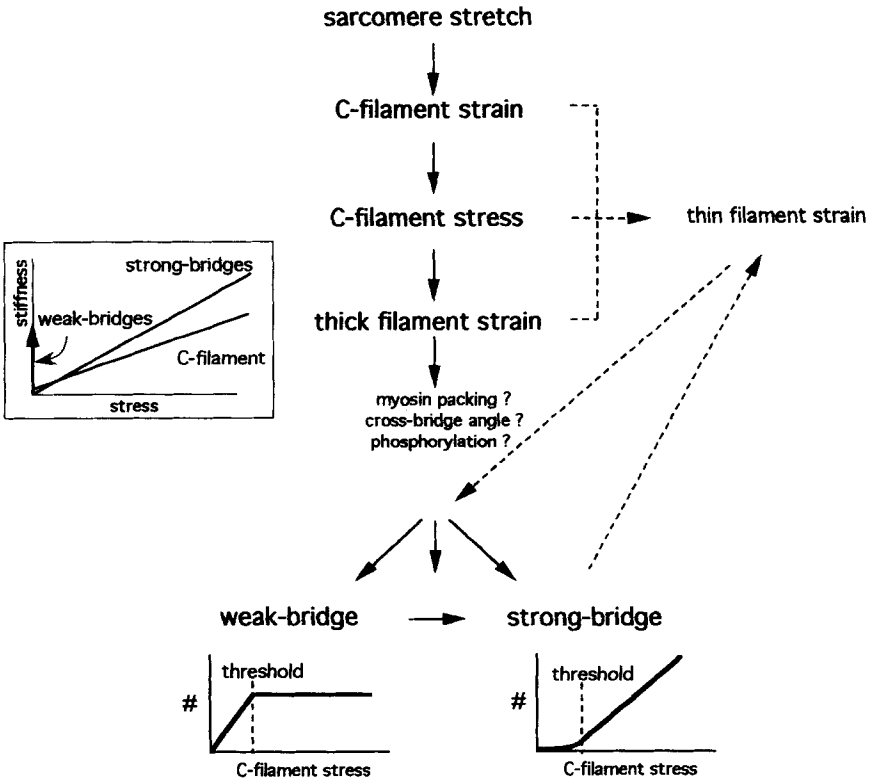

FIGURE 14. Working hypothesis for stress activation in indirect insect flight muscle. The C filament plays a dual role as sarcomere stretch sensor and stress generator. The C filament stress causes longitudinal strain on the thick filament, which in turn promotes the formation of both weak and strong cross-bridges. The number of weak bridges increases linearly with stress and reaches a plateau value at the stress threshold value. The number of strong bridges is small below this passive stress threshold and increases linearly with additional stress, presumably by conversion from weak bridges. Additional pathways (*dotted lines*) show the possible, but less likely, involvement of thin filament strain in the process. The inset shows the relation between stiffness and stress of weak bridges, strong bridges, and C filaments.

It is intriguing to speculate about the identity and behavior of the passive stress sensor that controls cross-bridge attachment. Proteins that either develop or bear passive stress are likely candidates. Since thin filament removal did not significantly affect passive stress (Fig. 8; Table II), thin filament proteins are unlikely to be

involved. Minititin is, however, a promising candidate. Minititin may respond to sarcomere stretch by extending and developing an elastic restoring force that strains the thick filament. A strained thick filament might display altered myosin packing and cross-bridge angle and altered levels of protein phosphorylation, thereby facilitating actomyosin interaction in both passive and active muscle. The proposed stress activation mechanism is presented schematically in Fig. 14.

In conclusion, it appears that in insect indirect flight muscle, passive and active tension are tightly coupled such that the number of force-generating cross-bridges during activation varies in direct proportion to passive tension before activation.

We are grateful to Dr. Michael Reedy for his advice in the earlier stage of this work and for his help in obtaining waterbugs. Dr. Marlena Kruger's help in purifying gelsolin is also highly appreciated. We thank the reviewers for their thoughtful and helpful comments.

This work was supported by grants from the Foundation for Research and the NIH (DK-20270) to K. Wang. H. Granzier acknowledges the support of a Neuromuscular Disease Research Fellowship from the Muscular Dystrophy Association of America.

Original version received 17 July 1992 and accepted version received 10 November 1992.

REFERENCES

Abbott, R. H., and P. E. Cage. 1984. A possible mechanism of length activation in insect fibrillar flight muscle. *Journal of Muscle Research and Cell Motility.* 5:387–397.

Ashhurst, D. E. 1977. The Z-line: structure and evidence for the presence of connecting filaments. *In* Insect Flight Muscle. R. T. Tregear, editor. Elsevier North-Holland Biomedical Press, Amsterdam. 57–73.

Ayme-Southgate, A., J. Vigoreaux, G. Benian, and M. L. Pardue. 1991. Drosophila has a twitchin/titin-related gene that appears to encode projectin. *Proceedings of the National Academy of Sciences, USA.* 88:7973–7977.

Barber, S. B., and J. W. S. Pringle. 1965. Functional aspects of flight in belostomatid bugs (Heteroptera). *Proceedings of the Royal Society of London, B.* 164:21–40.

Benian, G. M., J. E. Kiff, N. Neckelman, D. G. Moerman, and B. Waterston. 1989. Sequence of a large protein implicated in regulation of myosin activity in C. elegans. *Nature.* 342:45–50.

Brenner, B., J. M. Chalovich, L. E. Greene, E. Eisenberg, and M. Schoenberg. 1986. Stiffness of skinned rabbit psoas fibers in MgATP and MgPP solution. *Biophysical Journal.* 50:685–691.

Brenner, B., M. Schoenberg, J. Chalovich, L. Greene, and E. Eisenberg. 1982. Evidence for cross-bridge attachment in relaxed muscle at low ionic strength. *Proceedings of the National Academy of Sciences, USA.* 79:7288–7291.

Brenner, B., L. C. Yu, and J. M. Chalovich. 1991. Parallel inhibition of active force and relaxed fiber stiffness in skeletal muscle by caldesmon: implications for the pathway to force generation. *Proceedings of the National Academy of Sciences, USA.* 88:5739–5743.

Bryan, J. 1988. Gelsolin has three actin binding sites. *Journal of Cell Biology.* 106:1553–1562.

Bullard, B., K. Leonard, A. Larkins, G. Butcher, C. Karlik, and E. Fyrberg. 1988. Troponin of asynchronous flight muscle. *Journal of Molecular Biology.* 204:621–637.

Chalovich, J. M., L. C. Yu, and B. Brenner. 1991. Involvement of weak binding crossbridges in force production in muscle. *Journal of Muscle Research and Cell Motility.* 12:503–506.

Fabiato, A. 1988. Computer programs for calculating total from specified free or free from specified total ionic concentrations in aqueous solutions containing multiple metals and ligands. *Methods in Enzymology.* 157:378–417.

Funatsu, T., T. H. Higuchi, and S. Ishiwata. 1990. Elastic filaments in skeletal muscle revealed by selective removal of thin filaments with plasma gelsolin. *Journal of Cell Biology.* 110:53–62.

Goody, R. S., M. C. Reedy, W. Hofmann, K. C. Holmes, and M. K. Reedy. 1985. Binding of myosin subfragment 1 to glycerinated insect flight muscle in the rigor state. *Biophysical Journal.* 47:151–169.

Granzier, H., J. J. Lin, C.-L.A. Wang, and K. Wang. 1993. Effects of C-terminal caldesmon fragments on tension and stiffness of relaxed and activated asyncronous flight muscle. *Biophysical Journal.* In press. (Abstr.)

Granzier, H., J. Myers, and G. Pollack. 1987. Stepwise shortening of muscle fiber segments. *Journal of Muscle Research and Cell Motility.* 8:242–251.

Granzier, H., and K. Wang. 1993*a*. Gel electrophoresis of giant proteins: solubilization and silver-staining of titin and nebulin from single muscle fiber segments. *Electrophoresis.* In press.

Granzier, H., and K. Wang. 1993*b*. Selective removal of actin filaments with a non-calcium requiring gelsolin fragment (FX45). Effects on protein composition and mechanical properties of insect flight and vertebrate skeletal muscle. *Biophysical Journal.* (Abstr.) In press.

Granzier, H., J. Wiersma, R. Akster, and J. Osse. 1983. Contractile properties of a white- and a red-fibre type of the m.hyohyoideus of the Carp (*Cyprinus carpio L.*). *Journal of Comparative Physiology.* 149:441–449.

Higuchi, H., T. Suzuki, S. Kimura, S. Yoshioka, K. Maruyama, and Y. Umazuma. 1992. Localization and elasticity of connectin (titin) filaments in skinned frog muscle fibers subjected to partial depolymerization of thick filaments. *Journal of Muscle Research and Cell Motility.* 13:285–294.

Horowits, R., and R. Podolsky. 1987. The positional stability of thick filaments in activated skeletal muscle. Evidence for the role of titin filaments. *Journal of Cell Biology.* 105:2217–2223.

Hu, D. H., A. Mutsuno, K. Terakado, T. Matsuura, S. Kimura, and K. Maruyama. 1990. Projectin is an invertebrate connectin (titin): isolation from crayfish claw muscle and localization in crayfish claw muscle and insect flight muscle. *Journal of Muscle Research and Cell Motility.* 11:497–511.

Kawai, M., and P. W. Brandt. 1980. Sinusoidal analysis: a high resolution method for correlating biochemical reactions with physiological processes in activated skeletal muscles of rabbit, frog and crayfish. *Journal of Muscle Research and Cell Motility.* 1:279–303.

Kruger, M., J. Wright, and K. Wang. 1991. Nebulin as a length regulator of thin filaments of vertebrate skeletal muscle. Correlation of thin filament length, nebulin size and epitope profile. *Journal of Cell Biology.* 115:97–107.

Laemmli, U. K. 1970. Cleavage of structural proteins during the assembly of the head of bacteriophage T4. *Nature.* 227:680–685.

Lakey, A., C. Ferguson, S. Labeit, M. Reedy, A. Larkins, G. Butcher, K. Leonard, and B. Bullard. 1990. Identification and localization of high molecular weight proteins in insect flight and leg muscle. *European Molecular Biology Journal.* 9:3459–3467.

Maruyama, K. 1986. Connectin, an elastic protein of striated muscle. *International Review of Cytology.* 104:81–114.

Moss, R. L., M. R. Sollins, and F. R. Julian. 1976. Calcium activation produces a characteristic response to stretch in both skeletal muscle and cardiac muscle. *Nature.* 260:619–620.

Nave, R., D. Furst, U. Vinkemeier, and K. Weber. 1991. Purification and physical properties of nematode minititins and their relation to twitchin. *Journal of Cell Science.* 98:491–496.

Nave, R., and K. Weber. 1990. A myofibrillar protein of insect muscle related to vertebrate titin connects Z band and A band: purification and molecular characterization of invertebrate minititin. *Journal of Cell Science.* 95:535–544.

Pringle, J. W. S. 1965. Locomotion: flight. *In* The Physiology of Insecta. M. Rockstein, editor. Academic Press, New York. 283–329.

Pringle, J. W. S. 1977. The mechanical characteristics of insect fibrillar muscle. *In* Insect Flight Muscle. R. T. Tregear, editor. Elsevier North-Holland Publishing Company, Amsterdam. 177–196.

Pringle, J. W. S. 1978. The Croonian Lecture, 1977. Stretch activation of muscle; function and mechanism. *Proceedings of the Royal Society of London, B.* 201:107–130.

Reedy, M. K. 1971. Symposium on Contractility. R. J. Podolsky, editor. Prentice Hall, Englewood Cliffs, NJ. 229–246.

Reedy, M. K., K. R. Leonard, R. Freeman, and T. Arad. 1981. Thick filament mass determination by electron scattering measurements with the scanning transmission electron microscope. *Journal of Muscle Research and Cell Motility.* 2:45–64.

Schoenberg, M. 1988. Characterization of the myosin adenosine triphosphate (M.ATP) crossbridge in rabbit and frog skeletal muscle fibers. *Biophysical Journal.* 54:135–148.

Sobue, K., and J. R. Sellers. 1991. Caldesmon, a novel regulatory protein in smooth muscle and nonmuscle actomyosin systems. *Journal of Biological Chemistry.* 266:12115–12118.

Somerville, L., and K. Wang. 1981. The ultrasensitive silver protein stain also detects nanograms of nucleic acids. *Biochemical and Biophysical Research Communications.* 102:52–58.

Squire, J. M. 1981. The Structural Basis of Muscle Contraction. Plenum Publishing Corp., New York. 403–407.

Squire, J. M. 1986. Muscle: Design, Diversity and Disease. The Benjamin/Cummings Publishing Company, Inc. 159–162.

Squire, J. M. 1992. Muscle filament lattices and stretch-activation: the match-mismatch model reassessed. *Journal of Muscle Research and Cell Motility.* 13:183–189.

Thorson, J., and D. C. S. White. 1983. Role of cross-bridge distortion in the small-signal mechanical dynamics of insect and rabbit striated muscle. *Journal of Physiology.* 343:59–84.

Tregear, R. T. 1983. Physiology of insect flight muscle. *Handbook of Physiology.* 10:487–506.

Trinick, J. 1991. Elastic filaments and giant proteins in muscle. *Current Opinion in Cell Biology.* 3:112–118.

Trombitás, K., and A. Tigyi-Sébes. 1979. The continuity of thick filaments between sarcomeres in honey-bee flight muscle. *Nature.* 281:319–320.

Wang, K. 1985. Sarcomere-associated cytoskeletal lattices in striated muscle. *Cell and Muscle Motility.* 6:315–369.

Wang, K., R. McCarter, J. Wright, B. Jennate, and R. Ramirez-Mitchell. 1991. Regulation of skeletal muscle stiffness and elasticity by titin isoforms. *Proceedings of the National Academy of Sciences, USA.* 88:7101–7109.

Wang, K., R. McCarter, J. Wright, B. Jennate, and R. Ramirez-Mitchell. 1993. Viscoelasticity of the sarcomere matrix of skeletal muscles: the titin-myosin composite filament is a dual-range molecular spring. *Biophysical Journal.* In press.

White, D. C. S. 1983. The elasticity of relaxed insect fibrillar flight muscle. *Journal of Physiology.* 343:31–57.

White, D. C. S., and J. Thorson. 1973. The kinetics of muscle contraction. *Progress in Biophysics and Molecular Biology.* 27:175–255.

Wray, J. S. 1979. Filament geometry and the activation of insect flight muscle. *Nature.* 280:325–326.

Yamakawa, M., and Y. E. Goldman, 1991. Mechanical transients initiated by photolysis of caged ATP within fibers of insect fibrillar flight muscle. *Journal of General Physiology.* 98:657–679.